Enhanced CO2 Capture in Binary Mixtures of 1-Alkyl-3-methylimidazolium Tricyanomethanide Ionic Liquids with Water

ARTICLE *in* THE JOURNAL OF PHYSICAL CHEMISTRY B · SEPTEMBER 2013

Impact Factor: 3.3 · DOI: 10.1021/jp407364e · Source: PubMed

8 AUTHORS, INCLUDING:

G. E. Romanos
National Center for Scientific Research Demok…
90 PUBLICATIONS **1,030** CITATIONS
SEE PROFILE

Polycarpos Falaras
National Center for Scientific Research Demok…
215 PUBLICATIONS **6,663** CITATIONS
SEE PROFILE

Boyan Iliev
IoLiTec Ionic Liquids Technologies GmbH
30 PUBLICATIONS **147** CITATIONS
SEE PROFILE

Thomas Schubert
IoLiTec Ionic Liquids Technologies GmbH
56 PUBLICATIONS **921** CITATIONS
SEE PROFILE

THE JOURNAL OF PHYSICAL CHEMISTRY B

Article

pubs.acs.org/JPCB

Enhanced CO_2 Capture in Binary Mixtures of 1-Alkyl-3-methylimidazolium Tricyanomethanide Ionic Liquids with Water

George E. Romanos,*[,†] Lawien F. Zubeir,[‡] Vlassis Likodimos,[†] Polycarpos Falaras,[†] Maaike C. Kroon,[‡] Boyan Iliev,[§] Gabriela Adamova,[§] and Thomas J. S. Schubert[§]

[†]Institute of Advanced Materials, Physicochemical Processes, Nanotechnology and Microsystems-Division of Physical Chemistry, National Center for Scientific Research "Demokritos", Aghia Paraskevi Attikis, 15310 Athens, Greece

[‡]Separation Technology Group, Department of Chemical Engineering and Chemistry, Eindhoven University of Technology, Den Dolech 2, 5600 MB Eindhoven, Netherlands

[§]IoLiTec GmbH, Salzstrasse 184, 74076 Heilbronn, Germany

Supporting Information

ABSTRACT: Absorption of carbon dioxide and water in 1-butyl-3-methylimidazoliun tricyanomethanide ($[C_4C_1im][TCM]$) and 1-octyl-3-methylimidazolium tricyanomethanide ($[C_8C_1im][TCM]$) ionic liquids (ILs) was systematically investigated for the first time as a function of the H_2O content by means of a gravimetric system together with in-situ Raman spectroscopy, excess molar volume (V^E), and viscosity deviation measurements. Although CO_2 absorption was marginally affected by water at low H_2O molar fractions for both ILs, an increase of the H_2O content resulted in a marked enhancement of both the CO_2 solubility (ca. 4-fold) and diffusivity (ca. 10-fold) in the binary $[C_nC_1im][TCM]/H_2O$ systems, in contrast to the weak and/or detrimental influence of water in most physically and chemically CO_2-absorbing ILs. In-situ Raman spectroscopy on the IL/CO_2 systems verified that CO_2 is physically absorbed in the dry ILs with no significant effect on their structural organization. A pronounced variation of distinct tricyanomethanide Raman modes was disclosed in the $[C_nC_1im][TCM]/H_2O$ mixtures, attesting to the gradual disruption of the anion−cation coupling by the hydrogen-bonded water molecules to the $[TCM]^-$ anions, in accordance with the positive excess molar volumes and negative viscosity deviations for the binary systems. Most importantly, CO_2 absorption in the ILs/H_2O mixtures at high water concentrations revealed that the $[TCM]^-$ Raman modes tend to restore their original state for the heavily hydrated ILs, in qualitative agreement with the intriguing nonmonotonous transients of CO_2 absorption kinetics unveiled by the gravimetric measurements for the hybrid solvents. A molecular exchange mechanism between CO_2 in the gas phase and H_2O in the liquid phase was thereby proposed to explain the enhanced CO_2 absorption in the hybrid $[C_nC_1im][TCM]//H_2O$ solvents based on the subtle competition between the TCM−H_2O and TCM−CO_2 interactions, which renders these ILs very promising for CO_2 separation applications.

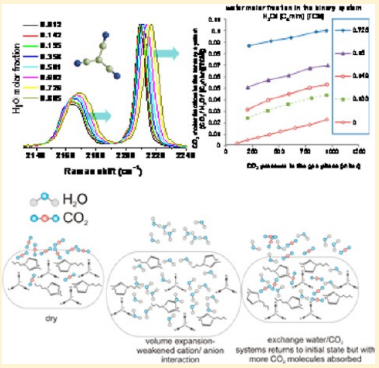

1. INTRODUCTION

Ionic liquids (ILs) have emerged as unique class of versatile solvents that holds great promise for a diverse range of technological applications and chemical processes,[1,2] a major one being their utilization as next-generation solvents for CO_2 capture.[3] Relying on their inherently low volatility and exceptional solvation capacity, intensive research efforts have been devoted to the development and engineering of suitable ILs that could supersede the volatile, corrosive, and energy-consuming amine-based solvents currently applied in CO_2 capture technology.[4−6] Binary IL/H_2O systems have been attracting particular attention as a promising and benign means to circumvent the impediment of the high ILs viscosity compared to traditional solvents and render feasible their practical application for CO_2 capture. The CO_2 absorption capacity of several IL/H_2O mixtures has been reported,[7−13] while molecular dynamics simulations have been applied in order to explore the influence of water on the CO_2 solubility and the underlying mechanism in the hydrated systems.[13,14] Stevanovic et al. showed that the presence of water in ILs interacting chemically with CO_2 such as the 1-alkyl-3-methylimidazolium acetates $[C_nC_1im][OAc]$ resulted in a marked decrease of the CO_2 absorption, despite the significant decrease of the ILs viscosity. Specifically, it was concluded that water not only hampers the IL-CO_2 chemical reaction but also lowers the physical solubility of the gas due to the competition between H_2O and CO_2 molecules at the same solvation sites.

Relying on the intrinsically selective and reversible reaction of CO_2 with aqueous amines (zwitterion mechanism), molecular design of the ILs structure by tethering an amine moiety to the cation[15] and more recently to the anion[16,17] resulted in a remarkable enhancement of the ILs capacity for

Received: July 24, 2013
Revised: September 12, 2013
Published: September 12, 2013

   dx.doi.org/10.1021/jp407364e | J. Phys. Chem. B 2013, 117, 12234−12251

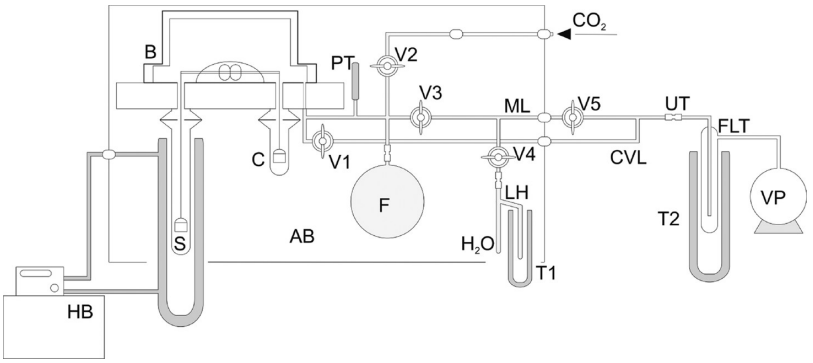

Figure 1. Gravimetric setup involved for conducting the CO_2 absorption experiments in ILs and H_2O/IL mixtures: (HB) constant temperature refrigerated/heating circulator, (F) high-volume flask, (LH) H_2O vessel, (FLT) foreline liquid nitrogen trap, (VP) mechanical vacuum pump, (UT) SS-316 Ultra-Torr connectors (Cajon), (PT) absolute pressure electronic transducer, (CVL) coarse vacuum line of the manifold, (ML) upper manifold line, (B) electronic microbalance head, (S) sample pan, (C) counterweight pan, (V1−V5) SS-316 diaphragm valves equipped with compressed air actuators.

CO_2 absorption from 1:2 to 1:1 CO_2:IL molar ratios. However, despite this marked progress in the CO_2 solubility, application of amine-functionalized ILs can be severely compromised by their high viscosities that increase dramatically (1−2 orders of magnitude) upon complexation with CO_2,[18−20] most likely due to formation of an extended IL/CO_2 hydrogen network.[21] This could be partly mitigated by judicious selection of the ILs anion[12,17] and the diluting effect of water that generally accelerates the CO_2 absorption rate[19] at the cost of a moderate decrease of the CO_2 absorption capacity.

In the case of physically absorbing ILs, whose CO_2 absorption capacity is determined by the physical solubity of CO_2 molecules in the void space within the liquid and the Lewis acid−base interaction of CO_2 with the anion,[22,23] the seminal work of Cammarata et al.[24] that was later corroborated by Danten et al.[25,26] using DFT calculations in combination with vibrational spectroscopy showed that water molecules preferentially interact with two anions leading to formation of nearly symmetric 1:2 H-bonded complexes of the form A···H−O−H···A. Early investigations by Aki et al.[7] showed that small amounts of water have a negligible effect on the solubility of CO_2 in 1-butyl-3-methylimidazolium bis-(trifluoromethylsulfonyl)imide [C_4C_1im][Tf_2N], suggesting that hydrogen bonding of water with the anion does not affect the anion−CO_2 interactions. Subsequent studies of tertiary IL/H_2O/CO_2 systems for anion fluorinated ILs at variable water contents and temperatures, namely, 1-butyl-3-methylimidazolium tetrafluoroborate [C_4C_1im][BF_4][8] and 1-butyl-3-methylimidazolium hexafluorophosphate [C_4C_1im][PF_6],[9] indicated that water has minor and/or weakly detrimental effects on the CO_2 solubility. More recently, Andanson et al., using attenuated total reflection (ATR) infrared spectroscopy on dry and wet [C_4C_1im][BF_4] and[C_4C_1im][PF_6] ILs at 313 K and pressures up to 150 bar of supercritical CO_2 ($scCO_2$), confirmed that water did not alter considerably the CO_2 solubility, while no significant effect could be detected on the interaction between the ILs anion and CO_2. A common feature threading these studies is that they all have been performed for ILs with fluorinated anions and for water molar fractions below 0.5, where rather weak effects of water on the CO_2 absorption were consistently established. This would further indicate that the hydrogen-bond basicity of the ILs and the strength of hydrogen bonding between IL anions and water do not correlate with their CO_2 absorption capacity.[7] Contradicting results were recently presented by Taib et al.,[11] who reported a higher absorption capacity in a 20% (w/w) IL solution in water ([C_4C_1im] [BF_4] and [bheaa] (bis(2-hydroxyethyl)ammonium acetate) that was attributed to the decrease of the solution viscosity and acceleration of the absorption rate.

In this work, a systematic investigation of the absorption of CO_2 and water was performed in 1-alkyl-3-methylimidazoliun tricyanomethanide ([$C_nC_1$im][TCM]) (n = 4, 8) that intrinsically possess several beneficial properties, i.e., low viscosity, low melting point, high thermal stability, and CO_2 solubility/selectivity together with scalable synthesis.[27−30] To this aim, a gravimetric system was applied for the first time in order to accurately determine the CO_2 absorption capacity and absorption kinetics of hybrid IL/H_2O solvents at different water contents, releasing the inherent limitations of the commonly employed isochoric saturation technique.[11,31,32] Specifically, formation of the mixed IL/H_2O solvent takes place in situ in the gravimetric system, providing higher precision in the determination of the H_2O molar fraction. Moreover, inaccuracies that may result due to water evaporation during the transfer of preweighted amounts of the hybrid IL/H_2O solvent or during equilibration into the measurement cell are avoided. Most importantly, the gravimetric system allows tracing the transient stage of sorption by monitoring the increase of mass rather than the drop of pressure. Thereby, it was possible to elucidate intriguing phenomena of exchange between H_2O in the liquid phase and CO_2 in the gas phase, pertinent to the [$C_nC_1$im][TCM]/H_2O system. Raman spectroscopy has been further employed to investigate the underlying interactions of both the binary [$C_nC_1$im][TCM]/CO_2 and [$C_nC_1$im][TCM]/H_2O mixtures as well as the tertiary [$C_nC_1$im][TCM]/H_2O/CO_2 systems. Thereby, a pronounced enhancement of both the CO_2 solubility and diffusivity in the mixed [$C_nC_1$im][TCM]/H_2O system was disclosed at high H_2O molar fractions. Relying on the Raman analysis together with excess molar volume (V^E) and viscosity deviation measurements, a molecular exchange mechanism based on the competition of H_2O and CO_2 with the tricyanomethnide anions was surmised to account for the distinctive behavior of the hydrated TCM ILs.

2. EXPERIMENTAL SECTION

2.1. Materials. The 1-butyl-3-methylimidazolium tricyanomethanide ([C_4C_1im][TCM]) and the 1-octyl-3-methylimida-

zolium tricyanomethanide ([C_8C_1im][TCM]) ionic liquids were prepared according to synthetic routes established in IoLiTech GmbH. Specifically, 1 mol of the corresponding imidazolium-based ionic liquid chloride (>98%, Iolitec) was dissolved in 1500 mL of dry dichloromethane. An amount of 1.05 mol of sodium tricyanomethanide was instantly added, followed by stirring for 48 h at room temperature. Subsequently, the mixture was filtered through Celite, the mother liquor evaporated under reduced pressure, and the product dried under high vacuum for 24 h at 313 K. Ionic chromatography showed Cl contents of below 1%, while the yields in both cases exceeded 90%. This procedure was further applied for synthesis of [C_2C_1Im][TCM] and [C_6C_1Im]-[TCM], for which complementary Raman spectroscopic measurements were performed. The water contents of the as-prepared ILs were determined by Karl Fischer titration to be 930, 720, 390, and 120 ppm for [$C_nC_1$im][TCM] with n = 2, 4, 6, and 8, respectively, reflecting the increased hydrophobicity of the TCM ILs with the increase of the alkyl chain length. The [C_nC_1Im][TCM] ILs thus combine the advantages of tunable hydrophobicity and low viscosity with scalable synthesis at a moderate cost compared to fluorinated anion ILs, which can fall well below 100 €/kg on a multiton scale. Absorption measurements were conducted using CO_2 (99.998%) gas.

2.2. Gravimetric System for CO_2 and H_2O Absorption. *Gravimetric Setup.* A schematic diagram of the apparatus developed for the performance of the experiments is shown in Figure 1. The measurement system (B) (CI MK2-M5 recording microbalance, CI PRESISION) is a force restoration, full beam, electronic microbalance with high capacity of 5 g load, 0.1 μg readability, and wide dynamic range (±1 g) that can operate from high vacuum up to 1.5 bar. The head (B) consists of a microbalance movement mounted on a rigid aluminum block which incorporates two hang-down ports and a vacuum/gas port.

The movement is of a double-sided construction, one side carrying the sample weight (S) and the other carrying the counterbalance weight (C). Both the sample and the counterweight are suspended from two rigid lattice arms, which allow uniform expansion at elevated temperatures. To minimize buoyancy effects, the construction materials of the hanging rods, pan carriers, weighing pans, and counterweight were appropriately selected for achieving almost identical bulk volumes of the several accessories hanged in the sample and counterweight compartments. Furthermore, a stainless steel manifold with diaphragm valves has been constructed and attached to the vacuum/gas port of the balance. The coarse vacuum line of the manifold (CVL) is used for outgassing the IL sample after being placed into the weighing pan, whereas the upper manifold line (ML) is used for CO_2 and H_2O vapor introduction into the balance and degassing water by successive melting/freezing cycles while vacuum pumping noncondensable gases through valve V4.

During water degassing valve V3 was kept closed in order to avoid contamination of the measurement section of the manifold with water vapor. Pressure is measured with an absolute pressure electronic transducer (PT), (WIKA 0−1250 mbar, and accuracy 0.02% full scale).

The sample compartment is maintained at constant temperature to within ±0.01 K via a double-walled glass vessel, with the thermal fluid (silicone oil) circulated by a JULABO (model MW12) constant temperature refrigerated/heating circulator (HP). A high-volume (2.5 L) borosilicate glass flask (F) is attached to the upper manifold line through valve V2 in order to avoid a drop of the pressure due to gas absorption by the IL or the IL/H_2O hybrid solvent. The balance head and measuring section of the manifold, enclosed between valves V1, V2, V4, and V5, were kept at ±0.1 K via an air bath, the temperature of which was controlled via an air-fan/resistance system and PID controller. Connection of the several glass components, e.g., the high volume flask (F), H_2O vessel (LH), and foreline liquid nitrogen trap (FLT) of the mechanical vacuum pump (VP), with the metal tubes was achieved by SS-316 Ultra-Torr (UT) connectors (Cajon). The valves of the system were SS-316 diaphragm valves equipped with compressed air actuators.

The valve control and readings of the balance, temperature, and pressure have been implemented via a homemade virtual instrument application, developed in LabView environment.

Measurement Procedure. To conduct the sorption experiments, small amounts of [C_4C_1im][TCM] and [C_8C_1im]-[TCM], (150 mg) were introduced in the weighing pan of the balance forming a liquid film of about 0.25 cm. Both ILs were outgassed at 353.15 K under high-vacuum (10^{-4} mbars) conditions, generated via a mechanical pump assisted by a foreline liquid nitrogen trap. All experiments were performed at 309.15 K in the following sequences.

For the case of [C_4C_1im][TCM], the CO_2 absorption/desorption isotherm was initially performed on the dry IL at several small pressure steps from 0 to 1 bar followed by outgassing of the sample (353.15 K, 10^{-4} mbars) and performance of a full H_2O absorption/desorption isotherm up to a relative vapor pressure of P/P_0 = 0.65. Then the sample was outgassed again at the same conditions (353.15 K, 10^{-4} mbars) and left to equilibrate at specific water vapor relative pressure. After mass relaxation (absorption equilibration) and without removing the water vapor from the measuring system, the sample was exposed sequentially at 5 different pressures of CO_2 from 0.2 to 1 bar. The sample was regenerated again and left to equilibrate at the next water vapor relative pressure. In this way, seven CO_2 absorption isotherms at 309.15 K have been performed after having exposed the sample at seven different water vapor relative pressures that corresponded to different H_2O molar fractions of the IL/H_2O hybrid solvent from 4×10^{-3} to 0.73. It has been concluded that water mass uptake obtained during the performance of the full H_2O absorption/desorption isotherm converged with this obtained in between the CO_2 sorption experiments of the IL/H_2O hybrid solvent.

In the case of [C_8C_1im][TCM] and in order to accelerate the analysis procedure the performance of a full water vapor absorption/desorption isotherm was omitted and the isotherm was reproduced from the water equilibration points obtained in between the CO_2 sorption experiments with the IL/H_2O hybrid solvent. The rest of the procedure was similar to that described for [C_4C_1im][TCM]. In this way, five CO_2 absorption isotherms at 309.15 K have been performed that corresponded to five different H_2O molar fractions of the IL/H_2O hybrid solvent from 4×10^{-3} to 0.57.

For the dry [C_4C_1im][TCM], mass relaxation at each CO_2 pressure step was achieved after a period of 22 h, while for [C_8C_1im][TCM] the required period was extended to 28 h. Water absorption was faster, and the mass relaxation time depended on the water vapor pressures.

Data Analysis. In gravimetric analysis there are two major issues of concern in order to assess correctly the solubility and diffusivity of CO_2 in ILs and IL/H_2O hybrid solvents. The first

Table 1. Mass and Density of the Several Components Involved in the Gravimetric Set Up

subscript	component	weight (mg)	material	density (g/cm^3)	temperature (K)
s	dry IL	m_s	$[C_4C_1im][TCM]$ or $[C_8C_1im][TCM]$	ρ_s (T_s, P)	T_s = 309.15 ± 0.01
s	IL/H_2O		$[C_4C_1im][TCM]/H_2O$ or $[C_8C_1im][TCM]/H_2O$		
1	wire upper part	42.11	stainless steel	7.972	T_c = 303.15 ± 0.1
i_1	wire lower part	39.45	stainless steel		309.15 ± 0.01
i_2	hook	3.64	stainless steel		
i_3	sample pan	267.90	aluminum	2.643	
j_1	hanging rod	45.02	stainless steel	7.972	303.15 ± 0.1
j_2	pan carrier	47.93	stainless steel		
j_3	counterweight pan	55.20	aluminum	2.643	
j_4	counterweight	227.10	Pyrex glass	2.230	-

is to apply the most accurate correction for the buoyant forces introduced due to gas pressure and temperature changes. The second has to do with volumetric changes of the binary IL/CO_2 and ternary IL/H_2O/CO_2 system due to the excess molar volume of the mixed IL/H_2O solvent and expansion upon CO_2 uptake. In the current work the static instead of the dynamic mode of operation was selected for performing analysis, and thereby other sources of error such as aerodynamic drag forces created by the flow of gases are negligible. Changes in the balance sensitivity due to changes in temperature can be also neglected since the balance head (electronics part) was maintained at ±0.1 K.

The equation applied for definition of the corrected mass uptake obtained from the microbalance was as follows

$$m_{cor} = m_{dis} - m_{dis,init} + \Delta m$$

$$\Delta m = \frac{m_s}{\rho_s(T_s, P)}\rho_g(T_s, P) + \frac{m_1}{\rho_1}\rho_g(T_c, P) + \sum_{i=1}\frac{m_i}{\rho_i}\rho_g(T_s, P) - \sum_{j=1}\frac{m_j}{\rho_j}\rho_g(T_c, P) \quad (1)$$

where m_{cor} is the corrected mass uptake, m_{dis} the display of the balance during gas uptake, $m_{dis,init}$ the initial display of the balance after outgassing, Δm the correction for buoyancy at each pressure (P), m_s/ρ_s the volume of the sample at several pressures (P) up to 1 bar and temperature T_s, m_1/ρ_1 the volume (stable) of the component of the weighing section at the temperature of the air bath T_c, m_i/ρ_i the volume (stable) of the several components of the weighing section at the temperature of the sample T_s, m_j/ρ_j the volume (stable) of the several components of the counterweight section at the temperature of the air bath T_c, and ρ_g (T,P) the density of the gas phase at a specific temperature and several pressures. Table 1 provides a list of each of the several components along with their weight, material of construction, density, and temperature.

The density of the dry ILs within a temperature range from 278.15 to 363.15 K was measured on an Anton Paar SVM 3000/G2-type stabinger with an uncertainty of ±0.0005 g/cm^3 and ±0.01 K for the temperature. The density of the IL/H_2O hybrid solvent at several water molar fractions was calculated from the excess molar volume results. The density of the IL/CO_2 and IL/H_2O/CO_2 systems at several pressures up to 1 bar and 309.15 K was considered as stable. It should be noted that attenuated total reflectance (ATR) Fourier transform infrared spectroscopy FT-IR measurements of IL/CO_2 and IL/H_2O/CO_2 systems in a special gastight, high-pressure cell are currently under way in order to define possible volume expansion and provide a more accurate calculation of the buoyancy effect. However, as already shown in previous investigations involving the FTIR technique, the volume expansion of the dry ILs upon CO_2 absorption up to a pressure of 1 bar is negligible.[33]

To investigate absorption kinetics, mass uptake data versus time were acquired from the sorption microbalance for each equilibrium pressure and temperature and corrected for buoyancy. For the definition of the binary diffusion coefficients, D (m^2·s^{-1}), of dissolved CO_2 and H_2O gases in the examined ILs, the transient curves of absorption (mass uptake vs time) were fitted to the appropriate solution for the transient absorption curve, holding for diffusion rate-controlled gas absorption in liquid films exhibiting one gas−liquid interface as it is in our case. The solution is derived from the transient diffusion equation according to a number of assumptions.

(1) Gas dissolves through a one-dimensional (vertical) diffusion process in which there is no convective flow in the liquid.
(2) A thin boundary layer between the gas and the liquid phases exists, where the thermodynamic equilibrium is instantly established with the saturation concentration and where the concentration is constant all the time at a given temperature and pressure.
(3) Temperature and pressure are kept constant.
(4) Uptake occurs over a small change in the absorbed phase concentration, and thereby constant diffusivity is assumed.
(5) Uptake within the absorbent sample is very small compared to the capacity of the system, which is implicitly valid in the Henry's law regime, i.e., for a very dilute absorbed phase.

The solution for the transient sorption curve is

$$\frac{m_t - m_0}{m_\infty - m_0} = 1 - \frac{8}{\pi^2}\sum_{n=0}^{\infty}\frac{1}{(2n+1)^2}\exp\left[-\frac{D(2n+1)^2\pi^2 t}{4l^2}\right] \quad (2)$$

where $m_t - m_0$ (mg) is the total amount of gas, which has diffused into the liquid film at time t (s), $m_\infty - m_0$ (mg) is the total amount of gas that has diffused into the liquid after infinite time, and l(cm) is the liquid film thickness. The diffusion coefficients for the several pressure steps were calculated according to eq 2 for a liquid film thickness, l, which was defined by the liquid mass and density and the diameter of the sample container used in the microbalance setup.

2.3. Excess Molar Volumes and Viscosity Measurements. For a deeper understanding of the effect of water on the thermophysical properties of the ILs, the excess molar

dx.doi.org/10.1021/jp407364e | J. Phys. Chem. B 2013, 117, 12234−12251

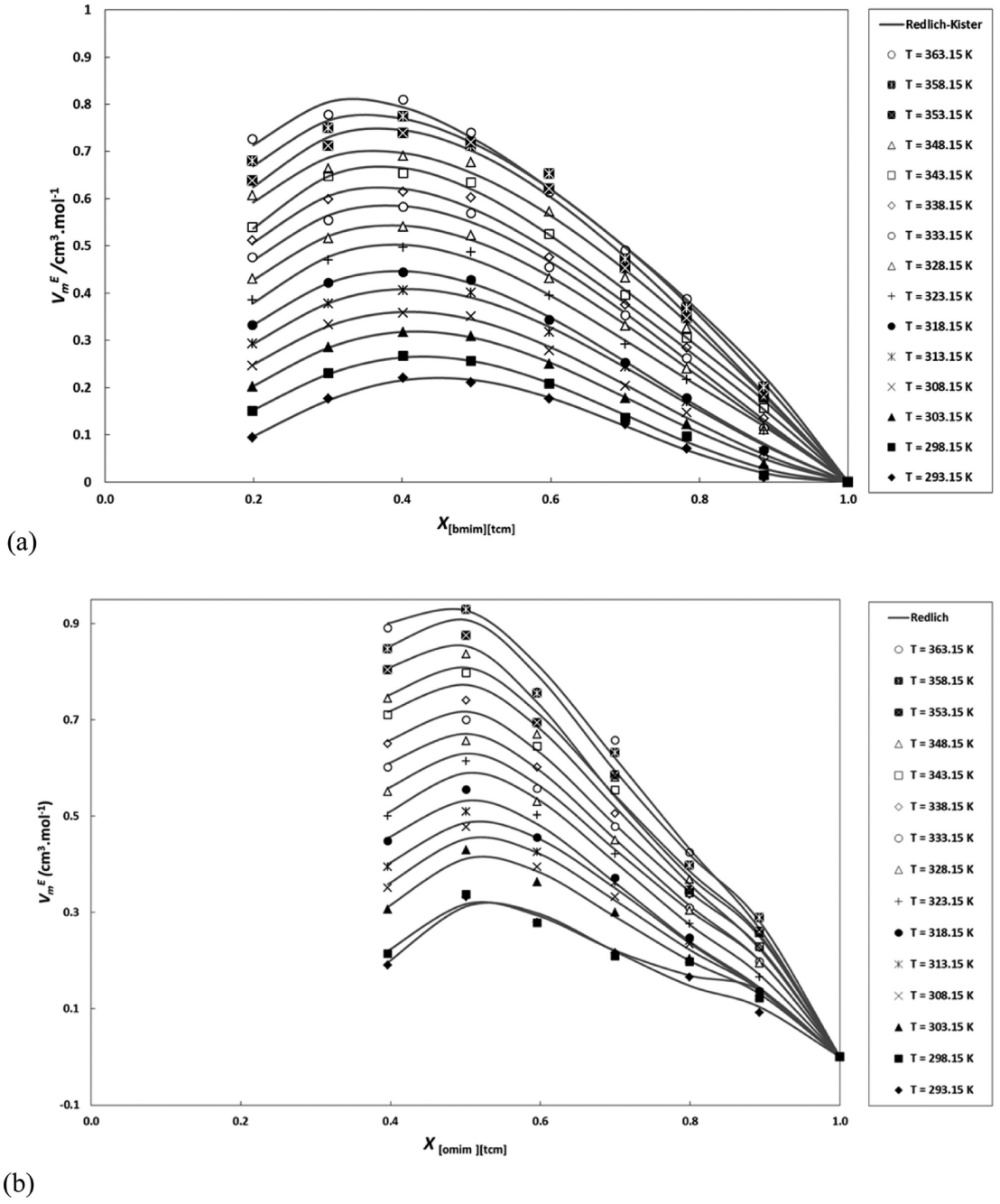

Figure 2. Excess molar volume of the binary systems (a) $[C_4C_1im][TCM]/H_2O$ and (b) $[C_8C_1im][TCM]/H_2O$ vs the IL mole fraction of at the indicated temperatures. Symbols represent experimental values, and the solid lines represent correlations using the Redlich−Kister expression with coefficients reported in Table S3, Supporting Information.

volume and viscosity deviations of the $[C_4C_1im][TCM]/H_2O$ and$[C_8C_1im][TCM]/H_2O$ systems were determined in the temperature range from 293.15 to 363.15 K at atmospheric pressure. Binary mixtures of IL and water were prepared by weighing the substances using a high-precision analytical balance (Sartorius CPA 3245, accuracy 1×10^{-4} g). Water used was treated with a Milli-Q water purification apparatus. This equipment provides ultrapure water through successive steps of filtration and deionization. Purity is expressed in terms of high resistivity (>18.2 MΩ·cm at 298.15 K) and particles size (<0.22 μm). Measurements of density and viscosity were performed using the Anton Paar SVM 3000, which determines both properties simultaneously. The viscometer has a dynamic viscosity range from 0.2 to 20 000 mPa·s and a density range from 0.65 to 3 g·cm^{-3}. The temperature uncertainty in the range from 288.15 to 378.15 K is ±0.02 K, the relative uncertainty of the dynamic viscosity is ±0.35%, and the absolute uncertainty in the density is 0.0005 g·cm^{-3}.

The thermophysical properties of the pure IL and its binary mixtures with water were described successfully using appropriate correlations. The dependence of density on temperature was described by a linear relation

$$\rho = A + B \cdot T \tag{3}$$

Here, A and B are the fitting parameters with B being the coefficient of the volume expansion (g·cm^{-3}·K).

dx.doi.org/10.1021/jp407364e | J. Phys. Chem. B 2013, 117, 12234−12251

Viscosities were correlated by means of the Vogel–Tammann–Fulcher equation

$$\ln(\eta) = A_\eta + \frac{B_\eta}{T/K - C_\eta} \quad (4)$$

where η is the viscosity (mPa·s), T is the temperature (K), and A_η, B_η, and C_η are adjustable parameters.

Moreover, after measuring the densities and viscosities of the pure components and of the binary liquid mixtures as a function of temperature and composition at atmospheric pressure, the excess molar volume and viscosity deviation from ideal mixture values were calculated. Excess molar volume was calculated using the following equation

$$V^E = \sum_{i=1}^{n} x_i M_i (\rho^{-1} - \rho_i^{-1}) \quad (5)$$

For a binary system eq 5 can be rewritten into

$$V^E = \frac{x_1 M_1 + x_2 M_2}{\rho_{mix}} - \frac{x_1 M_1}{\rho_1} - \frac{x_2 M_2}{\rho_2} \quad (6)$$

where V^E is the excess molar volume, M_i is the molar mass, x_i is the mole fraction of the ith component, ρ_{mix} is the density of the mixture, and ρ_i is the density of pure component i.

The dynamic viscosity deviation ($\Delta\eta$) for the mixtures was calculated using the following equation

$$\Delta\eta = \eta_m - \sum_{i=1}^{n} x_i \eta_i \quad (7)$$

where $\Delta\eta$ is the viscosity deviation (mPa·s) and η_m is the viscosity of the mixture.

The excess molar volumes and viscosity deviations were fitted using the Redlich–Kister expression.[34]

$$Y^E = x_1 x_2 \sum_{i=1}^{k} a_i (x_2 - x_1)^{i-1}$$
$$a_i = b_i + c_i \cdot T \quad (8)$$

Here, Y^E denotes V^E and $\Delta\eta$. b_i and c_i are fitting parameters attained by the least-squares root method, and k is the degree of polynomial expansion. The polynomial was truncated after four terms. Parameters were determined by a multiple-regression analysis based on the least-squares method. The corrected standard deviation of the fit is given by the following expression

$$\sigma = \sqrt{\sum_{i=1}^{n} \frac{(Y^E_{exp} - Y^E_{calcd})^2}{n - m}} \quad (9)$$

where n represents for the number of experimental points and m is the number of adjustable parameters.

2.4. Raman Spectroscopy. Raman spectra of the dry 1-alkyl-3-methylimidazolium TCM ILs and their binary mixtures with H_2O were recorded in backscattering configuration on a Renishaw inVia Reflex spectrometer using a near-infrared laser diode (λ = 785 nm) as the excitation source. The laser bean was focused on the sample by the ×5 objective of a Leica DMLM microscope connected to the Raman spectrometer. Rayleigh scattering was rejected with a 100 cm^{-1} cutoff dielectric edge filter, and analysis of the scattered beam was performed on a 250 mm focal length spectrometer along with a 1200 lines/mm diffraction grating and a high-sensitivity CCD detector. Subtraction of the luminescence background on the Raman spectra was performed by a polynomial fitting interpolation routine, while spectral deconvolution was carried out by nonlinear least-squares fitting of the Raman peaks to a mixture of Lorentzian and Gaussian line shapes, providing the peak position, width, height, and integrated intensity of each Raman band.

In-situ Raman measurements of the CO_2 dissolution in both the dry ILs and the binary IL/H_2O systems were performed at a temperature-controlled pressure cell (THMS600PS Linkam) that enables temperature- and pressure-dependent Raman measurement up to 14 bar over a wide temperature range (from −98 to 773 K). In these experiments, after loading the ionic liquid in a quartz crucible, the cell was initially outgassed at 323 K with N_2, then flashed with CO_2 to purge air and moisture, and then equilibrated at the desired temperature for 2 h. Subsequently, CO_2 was introduced in the cell under a typical pressure of 10 bar, and the solution was left to equilibrate for several hours while periodically recording the Raman spectra in intervals of 10 min until no spectral change could be observed.

3. RESULTS AND DISCUSSION

3.1. Excess Molar Volumes and Viscosity Deviations in the Binary IL/H_2O System. The excess properties as a function of temperature and composition provide information on the nonideality of the studied binary systems and hence the nature of the molecular interactions present in the mixture. The experimental excess molar volumes (V^E) calculated using eq 6 for the binary $[C_nC_1im][TCM]/H_2O$ systems at various temperatures are shown in Figure 2 and included in Table S1, Supporting Information, together with the experimentally determined densities of the pure components and of the binary mixture systems (Table S2, Supporting Information). The values of the Redlich–Kister coefficients are summarized along with the standard deviations between experimental and fitted data in Table S3, Supporting Information.

The binary systems show an immiscibility region at IL mole fractions between 0 and 0.2 for $[C_4C_1im][TCM]/H_2O$ and 0 and 0.4 for $[C_8C_1im][TCM]/H_2O$. Moreover, Figure 2 illustrates that the V^E is positive over the entire miscibility region for both ILs at the experimental conditions. Several factors may contribute to the positive value of V^E, like (1) disruption of the ordered molecular structure upon mixing within the liquid and the weakening or breaking of the strong ion–ion interactions resulting in a positive V^E [35] and (2) variations in molecular size (volume) and free volumes between the different components in the liquid mixture.[36] Unlike conventional solvents, room-temperature ILs based on alkylimidazolium cations present complex nanosegregation phenomena reflecting their local organization into polar and nonpolar domains determined by the interplay of strong electrostatic interactions between the positively charged imidazolium head and the anions and the van der Waals dispersion forces between the apolar alkyl tails.[37,38] Hydrogen bonding of water molecules with the ILs anion may gradually weaken the corresponding anion–ring interactions in the ILs/H_2O binary mixtures,[24] while growth of water clusters within the ILs polar network[39,40] would further screen and separate the anions leading to the nonmonotonous variation of the excess molar volume.[41] From Figure 2 it becomes clear that the curves are asymmetrical and that the maximum value of V^E can be found at an IL mole fraction of 0.4 and 0.5 for $[C_4C_1im][TCM]/H_2O$ and $[C_8C_1im][TCM]/H_2O$, respec-

dx.doi.org/10.1021/jp407364e | J. Phys. Chem. B 2013, 117, 12234–12251

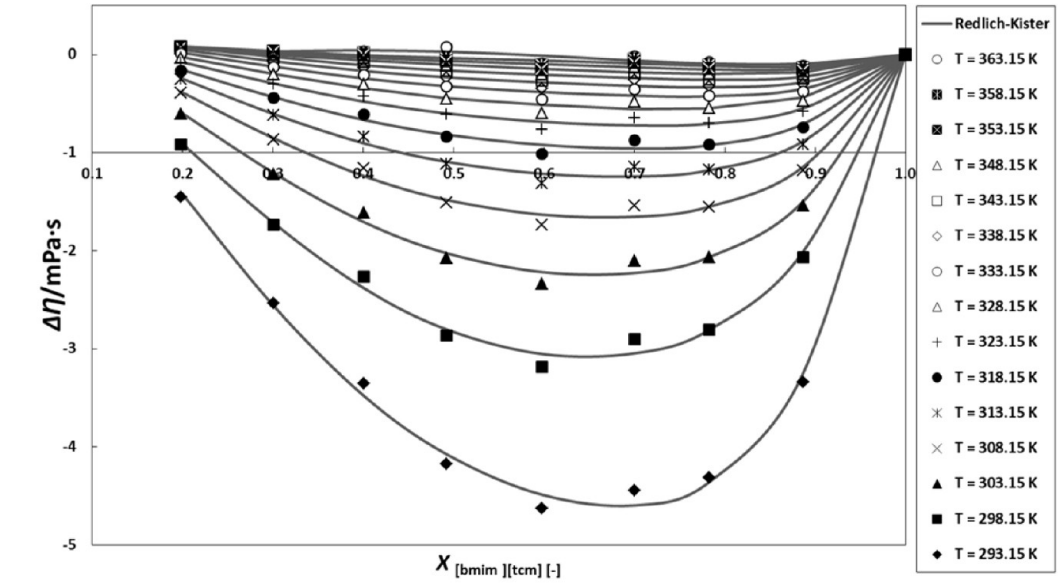

(a)

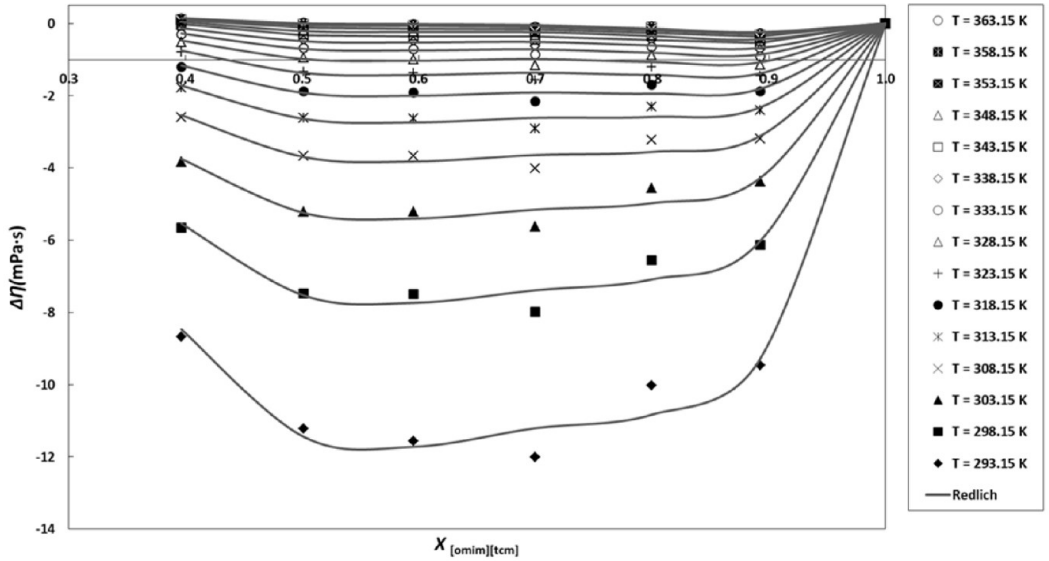

(b)

Figure 3. Viscosity deviations of the binary systems (a) $[C_4C_1im][TCM]/H_2O$ and (b) $[C_8C_1im][TCM]/H_2O$ vs the IL mole fraction at the indicated temperatures. Symbols represent experimental values, and solid lines represent correlations using Redlich–Kister expression with the coefficients reported in Table S4, Supporting Information.

tively. This suggests that a significant amount of water is needed to break the strong interactions of the IL.[41,42] Furthermore, V^E value increases with increasing temperature, which suggests that the mixture is more expandable than either of the individual compounds.

The experimental viscosity deviations ($\Delta\eta$) for the binary systems examined at various temperatures are presented in Figure 3. Unlike V^E, $\Delta\eta$ is negative over the entire miscibility region at the experimental conditions. A correlation between the signs of V^E and $\Delta\eta$ has been reported for a number of binary mixtures.[43,44] When V^E is positive $\Delta\eta$ is negative and vice versa. Negative $\Delta\eta$ values are associated with the presence of weak interactions or dispersion forces in mixtures with components having unequal size.[45] The decrease in the mixture viscosities implies the weakening of self-association through intermolecular hydrogen bonding in water and strong ionic interactions in the IL.

Data of the viscosity measurements of the pure components and $[C_nC_1im][TCM]/H_2O$ binary mixtures are given in Table S4, Supporting Information, whereas the data of the viscosity deviation $\Delta\eta$ and values of the Redlich–Kister coefficients summarized along with the standard deviations between experimental and fitted data are included in Tables S5 and S6, Supporting Information.

3.2. CO_2 and H_2O Absorption in the Dry ILs. Up to a pressure of 1000 mbars and at a temperature of 309.15 K, the absorbed molar fractions of CO_2, $X_{(CO2/(IL+CO2))}$, were limited below a value of 0.03 (Figure 4a), the absorption capacity was

dx.doi.org/10.1021/jp407364e | J. Phys. Chem. B 2013, 117, 12234–12251

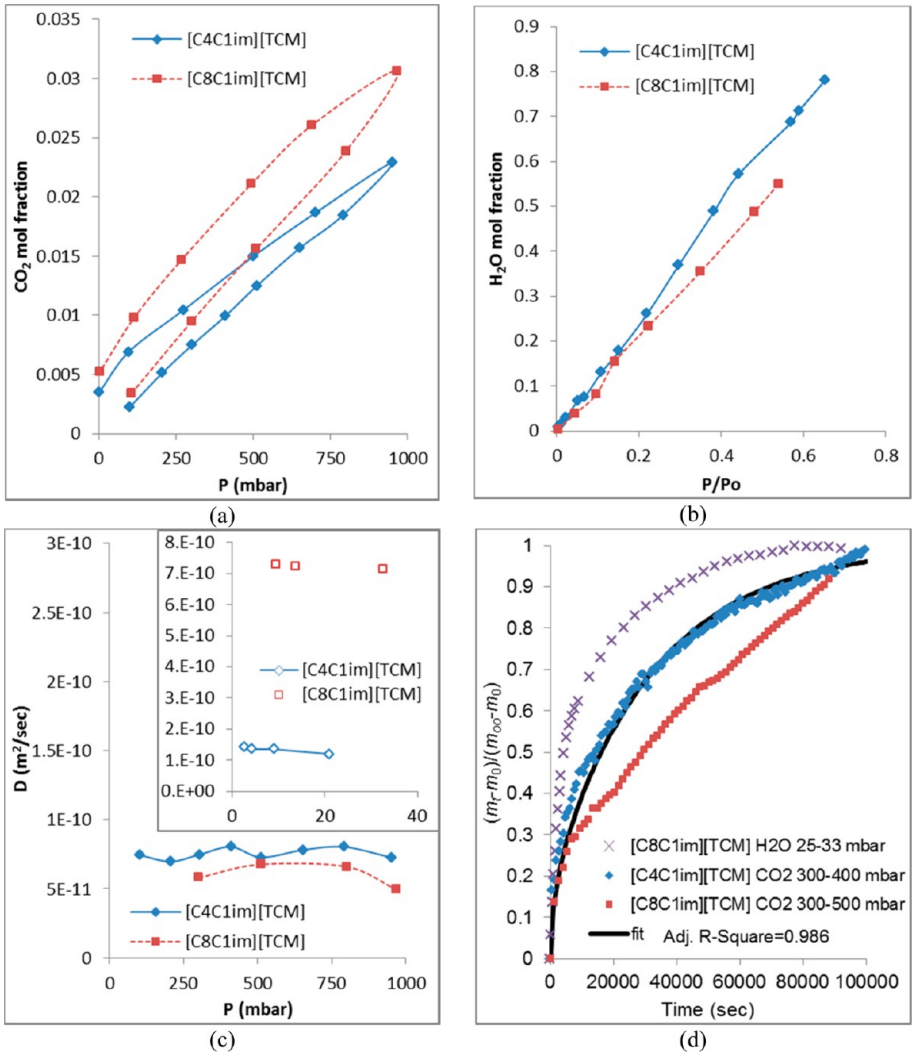

Figure 4. (a) Low-pressure absorption/desorption isotherms (309.15 K) of CO_2 in the examined ILs. (b) Water vapor absorption at 309.15 K in $[C_4C_1im][TCM]/H_2O$ and$[C_8C_1im][TCM]/H_2O$. (c) Binary diffusion coefficients (309.15 K) as a function of pressure for CO_2/IL and H_2O/IL (inset). (d) Representative transient absorption curves and respective fits of eq 2.

directly related to the imidazolium alkyl chain length, and the binary CO_2/IL diffusivity constants correlated inversely with the viscosity η (Table S4, Supporting Information) of the examined ILs (Figure 4c). Both ILs exhibited a small hysteresis in the desorption branch of the isotherm. However, upon return to high-vacuum conditions, most of the CO_2 had been desorbed without the need to increase the temperature of the sample, a behavior indicative of the physical nature of the interaction between CO_2 and the TCM ILs.

On the other hand, the water absorption capacity (Figure 4b) was very high, $X_{(H2O/(IL+H2O))}$= 0.61 and 0.51 for $[C_4C_1im][TCM]/H_2O$ and$[C_8C_1im][TCM]/H_2O$, respectively, at $P/P_0(H_2O)$ = 0.5 and correlated inversely with the alkyl chain length (hydrophobicity), while the water absorption rates were much faster compared to CO_2 (Figure 4c). Representative $(m_t - m_0)/(m_\infty - m_0)$ vs t plots for the studied ILs are depicted in Figure 4d, showing that CO_2 diffuses faster in $[C_4C_1im][TCM]/H_2O$ compared to $[C_8C_1im][TCM]/H_2O$ and that H_2O diffuses faster than CO_2 in $[C_8C_1im][TCM]/H_2O$, while the calculated diffusivities D ($m^2 \cdot s^{-1}$) as a function of pressure are presented in Figure 4c. It can be seen that due to the small pressure steps applied (small change of the gas concentration in the IL solvent) the binary diffusion coefficients are stable within the entire pressure range. A comparison of model to experiment for the mass transients, where diffusivity values are determined from the data fit, is presented in the Supporting Information (Figure S7).

3.3. CO_2 Absorption in the Binary System IL/H_2O.

Figure 5 shows the CO_2 absorption isotherms at 36 °C for the hybrid IL/H_2O solvents at several water molar fractions. Small concentrations of H_2O (up to a molar fraction $X_{(H2O/(IL+H2O))}$ of 0.008) in the hybrid IL/H_2O solvent did not have any significant effect on the CO_2 absorption efficiency. As already discussed in section 3.1, there is the need of high water amount in order to break the strong interactions of the ILs. In fact, inclusion of small amounts of water resulted in a small decrease of the CO_2 absorption capacity of the ILs, an effect that was more evident in the case of $[C_8C_1im][TCM]$ (Figure 5b) and could be explained in terms of the averaging between the CO_2 capture efficiencies of the two solvents (i.e., water and IL). In this regard, the relatively lower CO_2 absorption capacity of water as well as its negligible effect on the IL−CO_2 interaction at low concentrations led to a reduction of the CO_2-capturing efficiency of the hybrid solvent. On the other hand, an increase

dx.doi.org/10.1021/jp407364e | J. Phys. Chem. B 2013, 117, 12234−12251

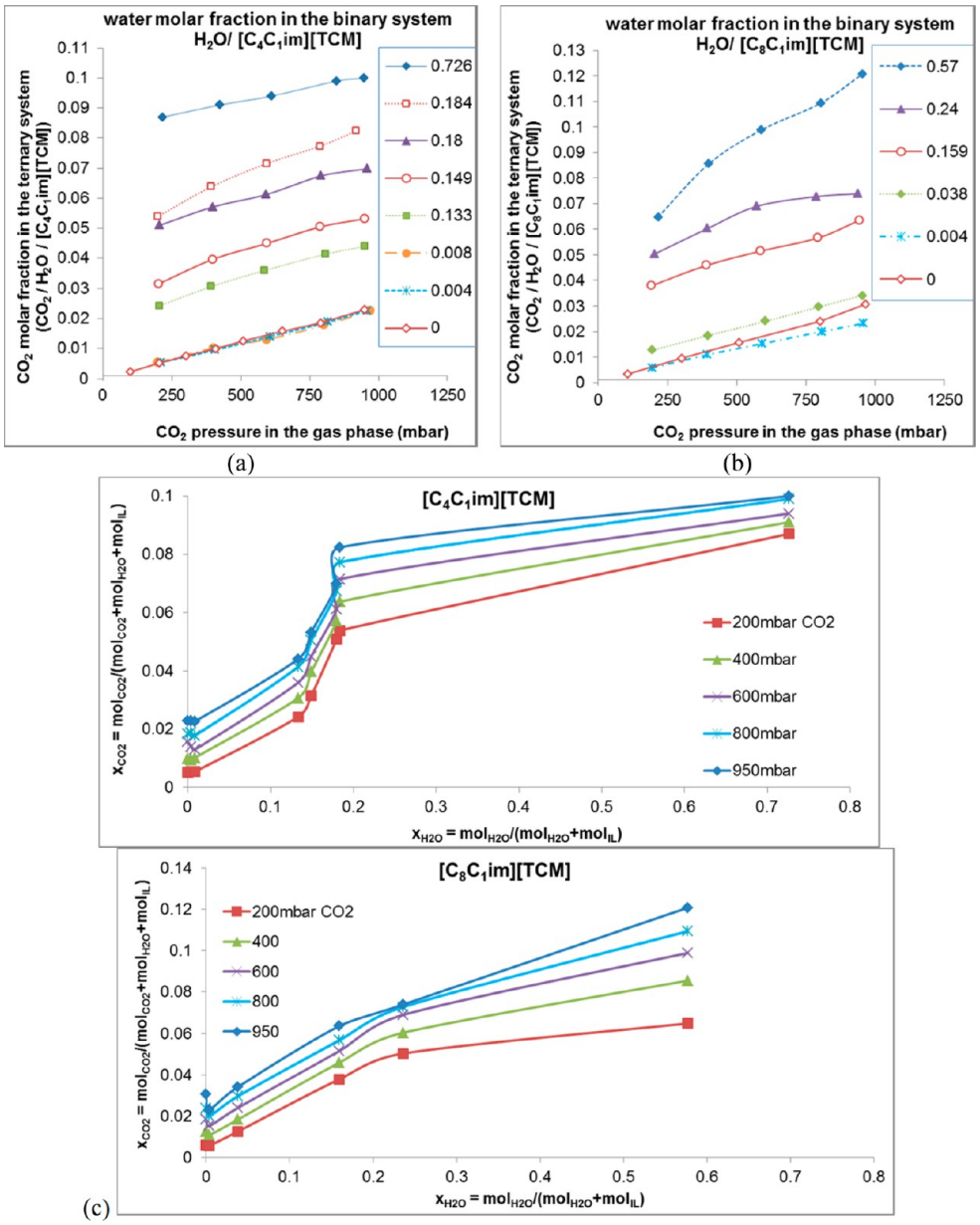

Figure 5. (a) CO_2 absorption isotherms at 36 °C in the hybrid $[C_4C_1im][TCM]/H_2O$ solvent at several water molar fractions. (b) Respective CO_2 isotherms for the $[C_8C_1im][TCM]/H_2O$ solvent. (c) Plots reproduced from a and b showing the dependence of the CO_2 capture efficiency on the water molar fraction at each CO_2 pressure.

of the water content resulted in a marked enhancement of the CO_2 absorption in the mixed $[C_nC_1im][TCM]/H_2O$ system compared to the dry ILs, in contrast to the insensitivity and/or detrimental influence of water on the CO_2 solubility for most chemically and physically absorbing ILs.[7−10,12,13] In the case of $[C_4C_1im][TCM]$, the positive effect of water on the CO_2 absorption emerged at water molar fractions above 0.12, leading to a significant enhancement of the CO_2 capture efficiency up to 4.5 times compared to the dry IL, over a narrow range of water concentrations ($X_{(H2O)/(IL+H2O)}$) = 0.12−0.2), as indicated in Figure 5c. The $[C_8C_1im][TCM]/H_2O$ hybrid solvent exhibited an almost linear dependence of the CO_2 capture efficiency as a function of the water molar fraction, possibly due to the less hydrophilic character of the involved IL. In that case, the CO_2 capture efficiency was enhanced up to 4 times compared to the dry IL at a water molar fraction of 0.57.

In the following paragraphs, a mechanism involving the exchange between CO_2 molecules in the gas phase and H_2O molecules in the liquid phase is proposed as the main reason underlying the enhanced CO_2 absorption capacity in the hybrid $[C_nC_1im][TCM]/H_2O$ solvents. Thus, it can be inferred that in the case of the more hydrophilic $[C_4C_1im][TCM]$ the exchange mechanism, e.g., breaking of the interaction between IL and H_2O molecules and replacement of H_2O with CO_2, is significantly enhanced when the concentration of water reaches a critical value.

It is also important to note (Figure 5a and 5b) that except for the case of $[C_8C_1im][TCM]$ at ($X_{(H2O)/(IL+H2O)}$) = 0.57, the slope of the CO_2 absorption isotherms of the hybrid IL/H_2O solvents for each water molar fraction is similar to that of the dry ILs. It becomes clear that most of the CO_2 absorptivity enhancement occurred within the first pressure step of 0−200 mbars, and as will be shown in the next section, it is at this

dx.doi.org/10.1021/jp407364e | J. Phys. Chem. B 2013, 117, 12234−12251

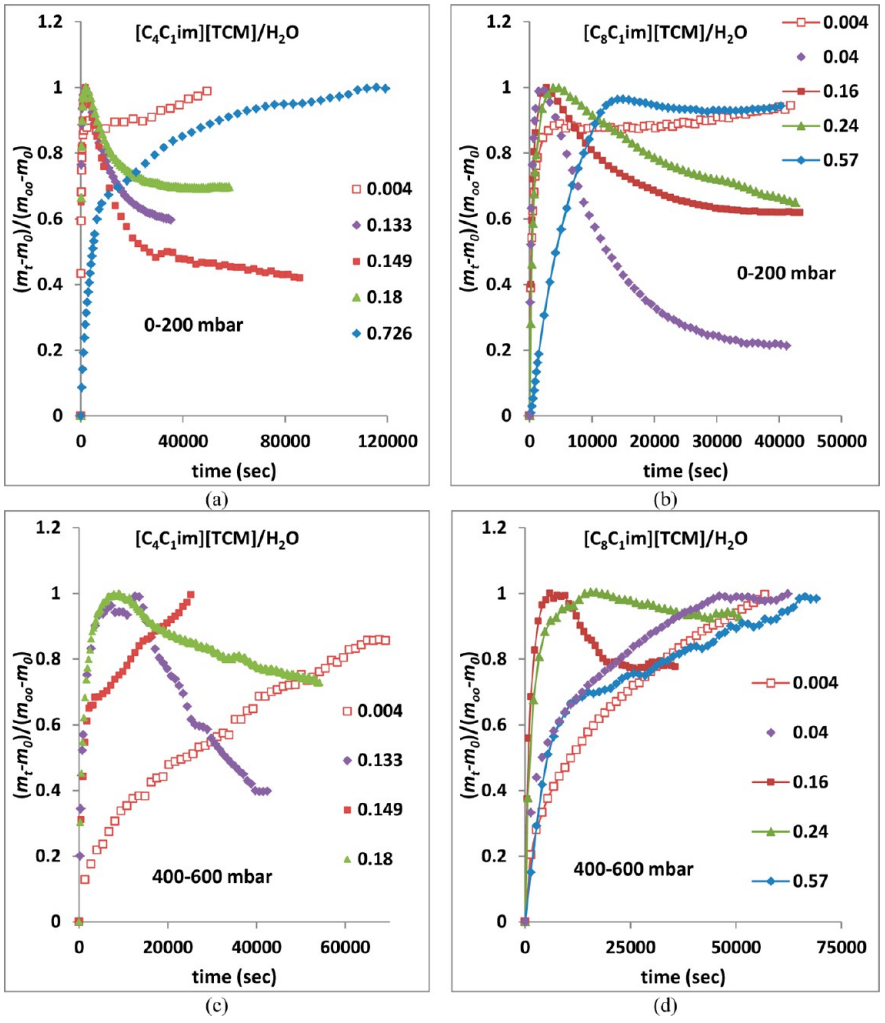

Figure 6. (a, c) CO_2 transients at pressure steps of 0−200 and 400−600 mbar at 36 °C for several water molar fractions in the hybrid $[C_4C_1im][TCM]/H_2O$ solvent. (b, d) CO_2 transients at respective pressure steps for several water molar fractions in the hybrid $[C_8C_1im][TCM]/H_2O$ solvent.

pressure step where the molecular exchange mechanism between water and CO_2 takes place.

3.4. Transient Stage of CO_2 Absorption in the Binary IL/H_2O System. The transient CO_2 absorption curves for the hybrid $[C_4C_1im][TCM]/H_2O$ and $[C_8C_1im][TCM]/H_2O$ solvents for pressure steps of 0−200 and 400−600 mbar for several H_2O molar fractions are presented in Figure 6. The shape of the transients, especially during the first pressure step (0−200 mbars) (Figure 6a and 6b), indicates that high amounts of CO_2 are initially absorbed in the hybrid solvent, and when the CO_2 concentration reaches a certain threshold, the absorbed CO_2 molecules weaken the interaction between the IL and H_2O, leading to the transfer of H_2O to the gas phase (desorption).

It should be stressed that the maximum in the mass uptake occurs half an hour to several hours after introducing the CO_2 dose into the gravimetric set up, and thus, it cannot be related with disturbances on the microbalance measuring system, which are usually caused by a sudden gas flow. Actually, the time needed to achieve an increase of the CO_2 pressure to the desired level never exceeded 1 min, and the accompanied balance disturbance is restricted to this short time period.

Another interesting remark is that the transient of CO_2 absorption in the hybrid solvents with the very low H_2O molar fractions is smooth and has the usual shape of CO_2 transients in the dry ILs for all applied pressure steps. The same holds for the high water molar fractions but with a distinctive difference between the $[C_4C_1im][TCM]/H_2O$ and the $[C_8C_1im]$-$[TCM]/H_2O$ hybrid solvents. As already mentioned in the previous section, in the case of the more hydrophilic $[C_4C_1im][TCM]$ the exchange mechanism, e.g., breaking of the interaction between IL and H_2O molecules, is possible only when the concentration of water reaches a critical value. Moreover, at high water concentrations a critical concentration of CO_2 is also needed to initiate H_2O desorption, expressed by a sudden mass decline during the last pressure step of 800−950 mbar (Figure S8e, Supporting Information). On the other hand, in the case of the less hydrophilic $[C_8C_1im][TCM]$, water desorption appears during the first pressure step of 0−200 mbar (Figure 6b), and the transient curves of the next pressure steps follow the usual uprising trend (Figure S8b,d,f, Supporting Information). Having a general view of the transient curves presented in Figure 6 and Figure S8, Supporting Information, it seems that the phenomena of water desorption are more frequent during the first pressure steps, although in some of the water molar fractions water desorption takes place up to the last CO_2 pressure step of 800−950 mbar.

dx.doi.org/10.1021/jp407364e | J. Phys. Chem. B 2013, 117, 12234−12251

Table 2. Comparison of Diffusivity Constants (D (m^2/s)) between the Dry IL and the Hybrid IL/H_2O Solvent at Low and High Water Molar Fractions

H_2O molar fraction in $[C_4C_1im][TCM]$ /H_2O						
pressure step (mbar)	0	0.004	0.008	0.149	0.18	0.726
0–200	6.97×10^{-11}			2.58×10^{-09}	2.96×10^{-09}	2.14×10^{-10}
200–400	7.475×10^{-11}	6.33×10^{-11}	1.66×10^{-10}			5.83×10^{-10}
400–600	8.04×10^{-11}	5.33×10^{-11}		1.22×10^{-09}		
600–800	7.282×10^{-11}		6.56×10^{-11}	1.82×10^{-09}	1.24×10^{-09}	8.25×10^{-10}
800–950	7.813×10^{-11}	4.53×10^{-11}	4.41×10^{-11}	8.1×10^{-10}		
H_2O molar fraction in $[C_8C_1im][TCM]$ /H_2O						
pressure step (mbar)	0	0.004	0.04	0.159	0.24	0.57
0–200						1.408×10^{-09}
200–400	5.82×10^{-11}	2.67×10^{-10}	1.179×10^{-09}	8.117×10^{-09}		5.563×10^{-10}
400–600	6.77×10^{-11}	4.68×10^{-10}	7.843×10^{-10}	4.435×10^{-09}		5.177×10^{-10}
600–800	6.60×10^{-11}	8.72×10^{-10}	5.23×10^{-10}	9.84×10^{-09}	1.34×10^{-09}	5.939×10^{-10}
800–950	4.95×10^{-11}	4.53×10^{-10}	2.448×10^{-10}	7.417×10^{-09}	6.95×10^{-10}	2.859×10^{-10}

The occurrence of a maximum and in general the shape of the transient curves precluded a good fit to the transient sorption equation (eq 2). However, at certain H_2O molar fractions it was possible to extract the binary diffusivity constants (D) and compare them with the corresponding ones for the dry solvents. The results (Table 2 and Figure 7)

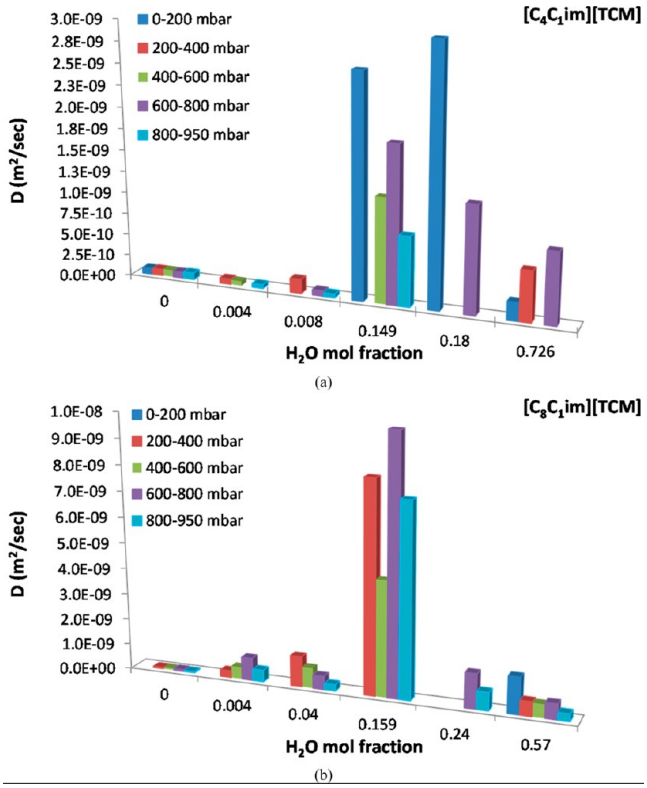

Figure 7. Binary CO_2/hybrid solvent diffusivity as a function of the water molar fraction for the different pressure steps for (a) $[C_4C_1im][TCM]$ and (b) $[C_8C_1im][TCM]$.

show considerable enhancement of the CO_2 diffusivity (1 order of magnitude), which when combined with the 4–5 times higher absorption capacity render the hybrid $[C_nC_1im][TCM]$/H_2O solvents very promising candidates for CO_2 capture applications. In particular, by examining Figures 5 and 7 it can be stated that the optimum CO_2 capture performance is attained for a water molar fraction of 0.2.

3.5. Raman Analysis of IL, IL/CO_2, IL/H_2O, and IL/H_2O/CO_2 Systems. *Raman Spectra of Dry TCM ILs.* Figure 8

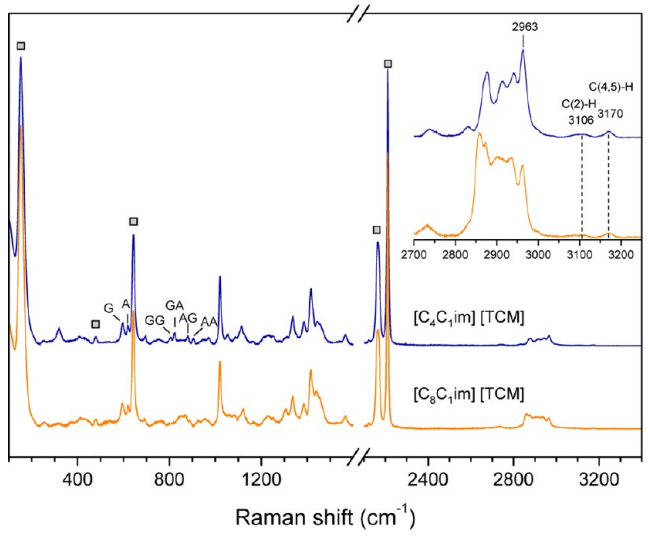

Figure 8. Raman spectra of the dry $[C_nC_1im][TCM]$ (n = 4 and 8) ILs. Squares depict the Raman modes of the tricyanomethanide anion. (Inset) Detailed CH vibration region for the two ILs.

compares the Raman spectra of the bare $[C_4C_1Im][TCM]$ and $[C_8C_1Im][TCM]$ ILs, where the discrete Raman modes reported for the 1-alkyl-3-methylimidazolium cations and their conformers can be identified.[46−50] In particular, the presence of four distinct Raman modes at 808, 825, 883, and 906 cm^{-1} verified the coexistence of the four combinations of gauche (G) and anti (A) conformers (GG, GA, AG, and AA) of the $[C_4C_1im]^+$ cation in the liquid state.[50] The bands at 324 and 975 cm^{-1} predicted for the GA/AA and AG/GG conformation states of $[C_4C_1im]^+$ have been also observed, along with the characteristic bands at 600, 624, and 699 cm^{-1} related to the contribution of the GG/GA, AG/AA, and GG/GA conformers, respectively.[50] The latter three modes were also identified in $[C_8C_1im][TCM]$, indicating that this type of isomerism is a common feature of the long alkyl-chain methylimidazolium cations.[47] An additional band was observed at 1309 cm^{-1} for $[C_8C_1im][TCM]$, which has been assigned to

dx.doi.org/10.1021/jp407364e | J. Phys. Chem. B 2013, 117, 12234−12251

the combination mode of the in-plane imidazolium ring bending with chain twisting CH_2 vibrations.[47,51]

Identification of the $[C_nC_1Im]^+$ cation vibrational modes allowed discriminating the tricyanomethanide anion Raman bands, in accordance with relevant Raman studies of TCM salt.,[52−54] Five distinct Raman bands were accordingly identified for $[TCM]^-$ anions (Table 3), comprising the intense in-plane CCN bending mode at 159 cm^{-1}, the weak out-of-plane CCN bend at 483 cm^{-1}, and the strong symmetric CC and CN stretching modes at 646 and 2209 cm^{-1}, respectively, together with an inhomogeneously broadened band at 2164 cm^{-1}, assigned to the antisymmetric CN vibration (vide infra). Comparison of the corresponding peak positions with those reported for the free $[TCM]^-$ anions in solution, where a D_{3h} planar symmetry has been consistently derived,[52,53] shows a significant red shift (softening) of the CC and CN stretches upon coupling with the $[C_nC_1im]^+$ cations, while the bending mode frequencies are slightly affected (Table 3). This suggests that the specific modes are appreciably weaker in the ionic liquid state, providing direct evidence for the restricted vibrational motion along the C−C−N axis for $[TCM]^-$ ions upon coupling with the 1-alkyl-3-methylimidazolium cations.

Furthermore, comparison of the $[C_4C_1im][TCM]$ and $[C_8C_1im][TCM]$ Raman spectra in the CH vibration region (2700−3200 cm^{-1}) revealed marked variations of the alkyl chain CH stretching modes (below 2950 cm^{-1}), as shown in the inset of Figure 8. Specifically, an increase of the number of methylene groups for $[C_8C_1im][TCM]$ resulted in the shift and intensification of the corresponding CH stretches toward lower frequencies due to the contribution of additional modes from the longer alkyl chains. On the other hand, the higher frequency CH mode at 2963 cm^{-1}, attributed to the terminal methyl group of the imidazolium ring,[47] was least affected by the alkyl chain length. Likewise, the CH stretches associated

Table 3. Raman Modes of $[TCM]^-$ Anions in $[C_nC_1im][TCM]$ Compared to Those of the Free Ions[a]

ν (cm^{-1})			
$[C_nC_1im][TCM]$	free $[TCM]^-$	$\Delta\nu$ (cm^{-1})	assignment (D_{3h})
159	159(1)	1(1)	in-plane C−C−N bending (E′)
483	484	1	out-of-plane C−C−N bending (E″)
646	657(1)	11(1)	symmetric C−C stretching (A_1')
2164	2174(1)	10(1)	antisymmetric C−N stretching (E′)
2209	2224(1)	16(1)	symmetric C−N stretching (A_1')

[a]Frequencies and symmetry assignments for free $[TCM]^-$ anions by Hipps and Aplin[52] and Dixon et al.[53]

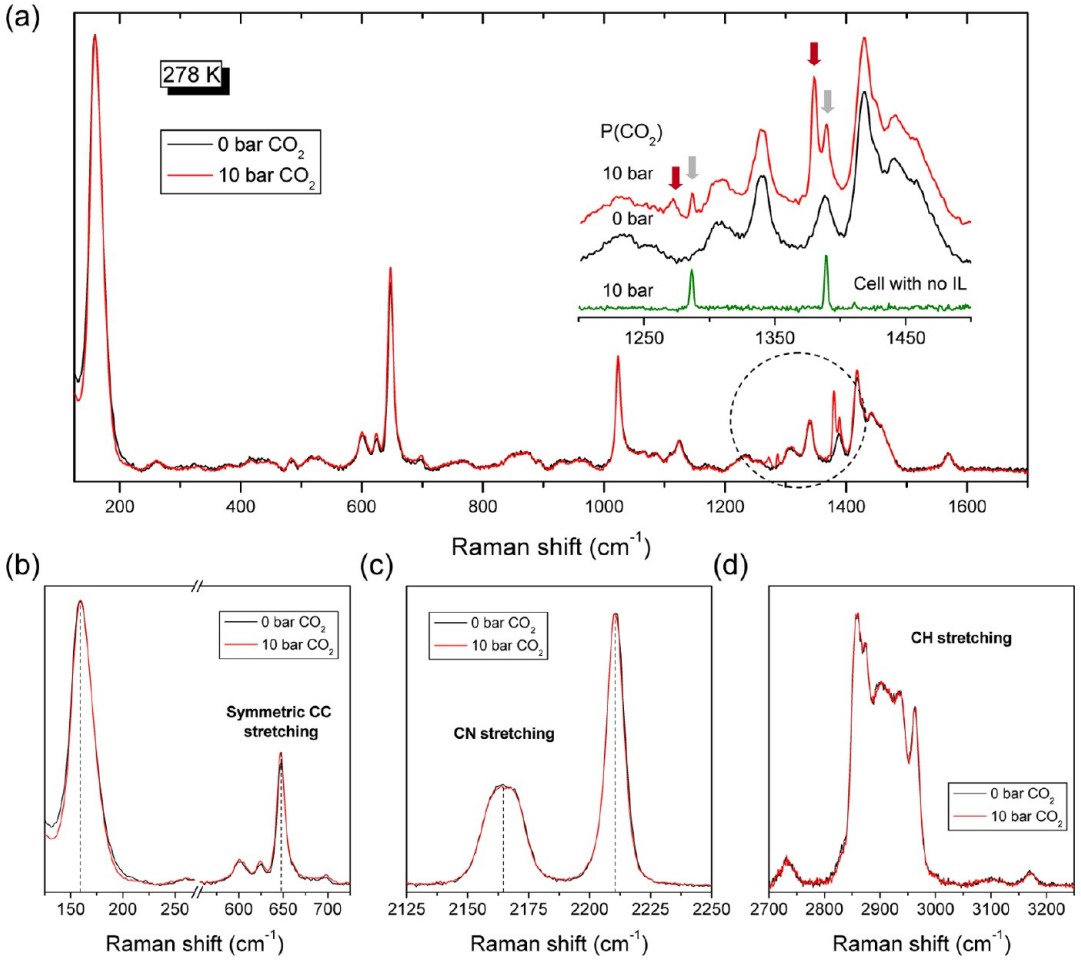

Figure 9. Raman spectra of $[C_8C_1im][TCM]$ before (0 bar) and after absorption of CO_2 under pressure of 10 bar at 278 K at different spectral regions. (Inset) Detailed frequency range of 1200−1500 in comparison with the Raman spectrum of the empty cell filled with CO_2 at 10 bar. Two pairs of Fermi dyads are depicted by dark and light arrows.

dx.doi.org/10.1021/jp407364e | J. Phys. Chem. B 2013, 117, 12234−12251

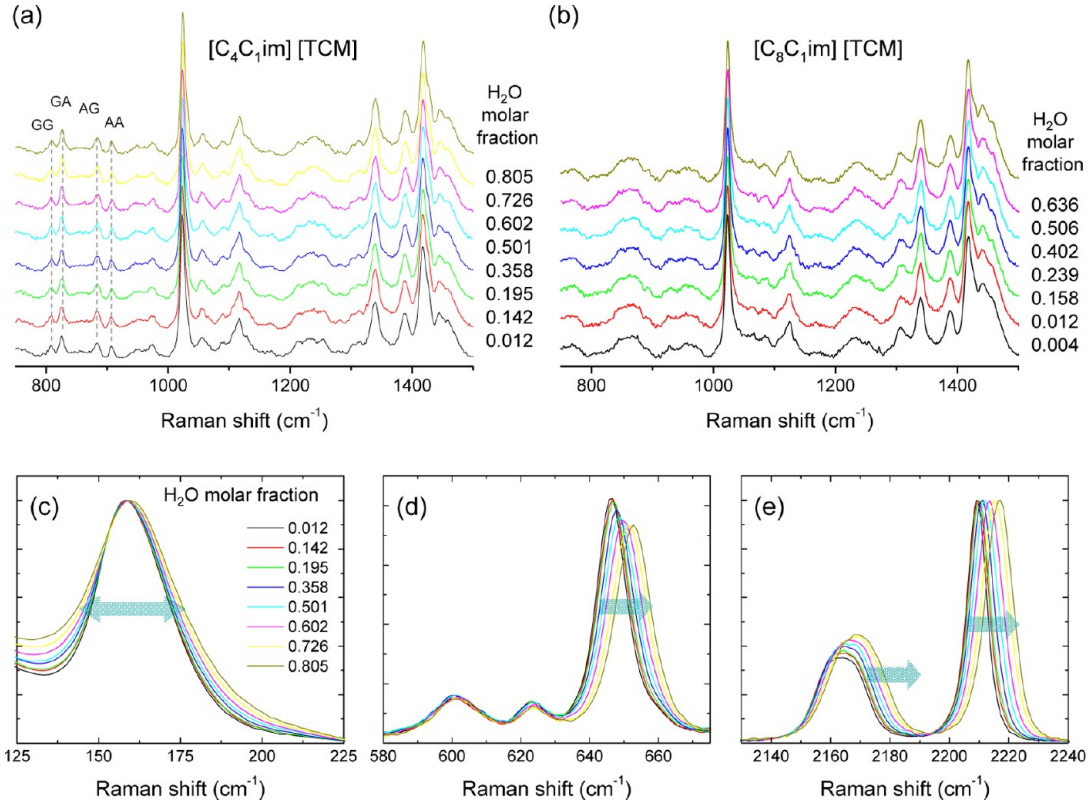

Figure 10. Raman spectra for the binary (a) $[C_4C_1im][TCM]/H_2O$ and (b) $[C_8C_1im][TCM]/H_2O$ mixtures as a function of the water molar fraction in the spectral region of 750−1500 cm^{-1} dominated by the $[C_nC_1im]^+$ modes. Evolution of the (c) in-plane CCN bending, (d) CC, and (e) CN stretching modes of $[TCM]^-$ anions with the water concentration for $[C_4C_1im][TCM]/H_2O$.

with the NC(2)HN and HC(4)C(5)H groups of the imidazolium ring were observed as a broad band centered at 3106 cm^{-1} and a narrower and more intense one at 3170 cm^{-1}, respectively, for both ILs. The frequencies of these modes, which are considered to reflect most sensitively the anion−cation coupling,[47,55,56] were close to those reported for anion fluorinated ILs, namely, ∼3120 and ∼3180 cm^{-1} for $[C_4C_1im][PF_6]/[C_4C_1im][BF_4]$[46,48] and 3097 and 3165 cm^{-1} for $[C_4C_1im][COOCF_3]$,[57] implying comparable interaction strength.

Binary TCM IL/CO_2 Mixtures. Subsequently, in-situ Raman measurements of CO_2 dissolved in the TCM ILs have been carried out at constant temperatures in order to explore and classify the IL−CO_2 interaction. Figure 9a displays the Raman spectra of $[C_8C_1im][TCM]$ before and after equilibration under a CO_2 pressure of 10 bar at 278 K. Neither the cation nor the anion modes was thus found to be appreciably affected by the absorption of CO_2 in the ionic liquid, as illustrated for some pertinent spectral regions in Figure 9b−d. No effect could be accordingly traced on the $[TCM]^-$ modes or the cation CH stretches in the applied pressure range (0−10 bar), indicative of a relatively weak IL−CO_2 interaction with no major perturbation of the IL's structure.[10,22] The only notable effect was detected in the spectral range of 1250−1400 cm^{-1}, where two pairs of narrow Raman bands evolved upon CO_2 absorption, as depicted in the inset of Figure 9a, characteristic of two distinct CO_2 Fermi resonance dyads.[58] The narrower dyad peaks at 1285 and 1389 cm^{-1}, marked with gray arrows in the inset of Figure 9a, emerged immediately after introducing the pressurized CO_2 in the Raman cell containing the ionic liquid. These modes were readily identified to stem from gas CO_2 molecules in the void space above the sample holder by comparative measurements in the Raman cell under the same CO_2 pressure (10 bar) with no IL. The observed frequencies matched those of the CO_2 Fermi dyad in the gas phase,[58] and the corresponding spectrum has been accordingly utilized as an internal reference for CO_2 dissolution. On the other hand, the second pair of Raman peaks evolved gradually during equilibration of the IL/CO_2 system and was shifted to appreciably lower frequencies, 1272 and 1380 cm^{-1}, compared to those of gas CO_2 molecules. This Fermi dyad has been accordingly assigned to CO_2 molecules dissolved in the ionic liquid.

Additional Raman experiments were performed for the $[C_8C_1im][TCM]$−CO_2 binary system at lower temperatures, namely, 248, 263, and 273 K, under 10 bar of CO_2 pressure (Figure S1, Supporting Information), where the absence of any distortion of the anion/cation Raman bands was also evidenced. On the other hand, the relative intensity of the CO_2 Fermi dyad increased systematically upon lowering temperature, quantified by the intensity ratio I_{1380}/I_{646} calculated from the area of the 1380 cm^{-1} Fermi peak to that of the $[TCM]^-$ symmetric CC stretch at 646 cm^{-1} (Figure S2, Supporting Information), indicating an enhancement of the CO_2 solubility with no noticeable distortion of the IL's structure.

This was further corroborated by complementary Raman measurements on $[C_nC_1im][TCM]$ (n = 2, 4, 6) ILs as a function of the alkyl chain length at a constant temperature of 263 K and CO_2 pressure of 10 bar. Similar to the octyl analogue, no modification of the anion/cation Raman bands could be detected for the TCM ILs with shorter alkyl chains

dx.doi.org/10.1021/jp407364e | J. Phys. Chem. B 2013, 117, 12234−12251

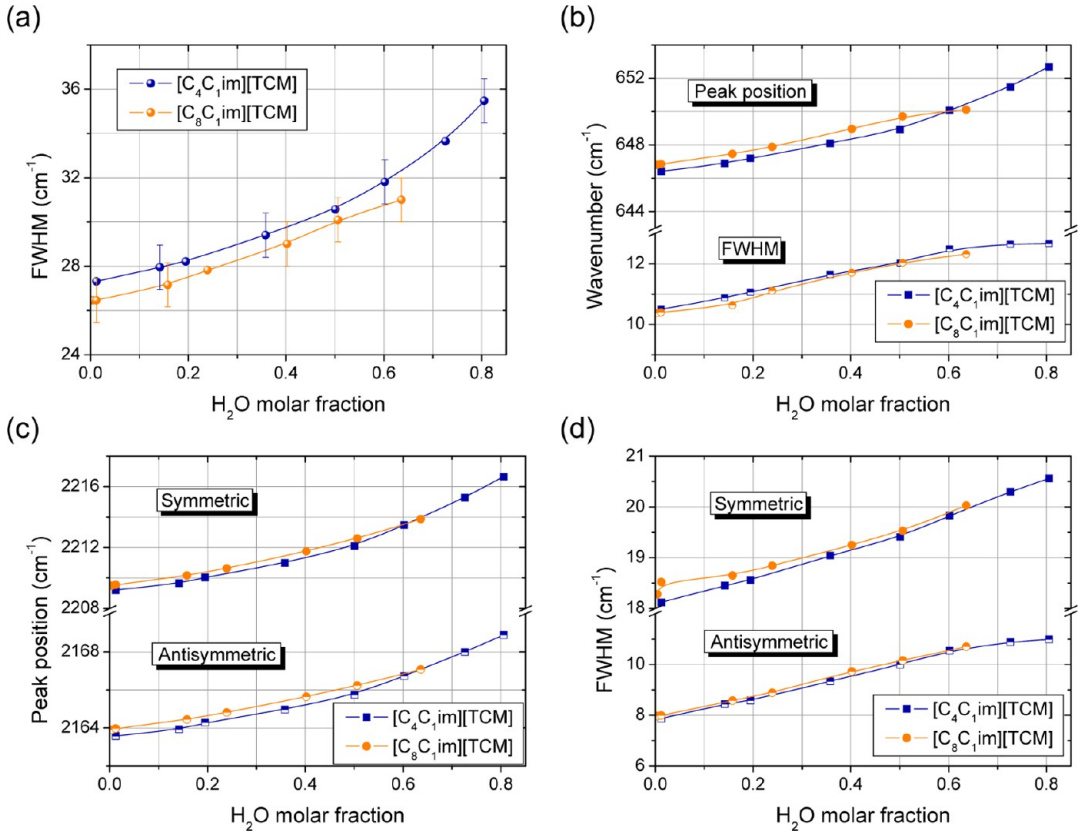

Figure 11. Water dependence of the (a) full-width at half-maximum (fwhm) of the in-plane CCN bending, (b) peak position and fwhm of the symmetric CC stretching, and (c) peak position and (d) fwhm of the symmetric and antisymmetric CN stretching modes for the $[C_4C_1im][TCM]/H_2O$ and $[C_8C_1im][TCM]/H_2O$ binary systems.

(Figure S3, Supporting Information). Plotting the relative intensity of the CO_2 Fermi dyad (I_{1380}/I_{646}) revealed a linear increase of the corresponding area ratio with the alkyl chain length (Figure S4, Supporting Information) and thus of the CO_2 solubility complying favorably with the corresponding free volume expansion with the increase of the alkyl chain,[7] a characteristic feature of physical CO_2 absorption.[6]

Regardless of the intensity differences caused by temperature variations or the alkyl chain, the positions of the Fermi dyad peaks remained constant at 1272 and 1380 cm^{-1} for all the TCM ILs, implying a common interaction mechanism with CO_2. Moreover, the observed Fermi dyad frequencies were close, though lower than those reported by Raman measurements for H_2O dissolved in H_2O (1277 and 1384 cm^{-1})[58] as well as in $[C_2C_1im][BF_4]$ (1278 and 1384 cm^{-1}) and $[C_2C_1im][Tf_2N]$ (1279 and 1384 cm^{-1}) fluorinated ILs,[59] pointing to a relatively stronger interaction of CO_2 with the TCM ILs. Recently, a thorough study of the CO_2 interaction with $[C_4C_1im][COOCF_3]$ by means of in-situ Raman spectroscopy under high CO_2 pressure (1−90 bar) in the supercritical regime (313 K)[57] showed that the Raman modes of the ionic liquid were essentially unaffected by the CO_2 dilution, except for a weak enhancement of the symmetric COO^- stretch of the trifluoroacetate anion at high pressures. Moreover, line shape analysis of the CO_2 Fermi dyad revealed the superposition of two pairs of CO_2 Fermi dyads, pointing to the presence of CO_2 in two different environments. The high-frequency Fermi dyad was accordingly attributed to CO_2 molecules accommodated in the free space of the IL interacting with themselves, while the low-frequency one was related to CO_2 interacting weakly with the negatively charged COO group of the anion.[57] The positions of the low-frequency Fermi dyad were at ∼1272 and ∼1381 cm^{-1} at low (∼0.2) CO_2 molar fractions, very close to the positions of the Fermi dyad identified in the TCM ILs. This would further imply that although no significant distortion of the TCM ILs Raman bands could be traced in the applied pressure range, weak specific interactions of CO_2 with the TCM anion may also occur,[22] which is mainly reflected on the shift of the CO_2 Fermi dyad modes rather than the anion Raman modes.

Binary TCM IL/H_2O Mixtures. Raman spectroscopy was further applied to investigate the effect of water and the underlying interactions in binary IL/H_2O mixtures within the miscibility region. Figure 10a and 10b shows an overview of the $[C_4C_1im][TCM]/H_2O$ and $[C_8C_1im][TCM]/H_2O$ Raman spectra as a function of the H_2O molar fraction in the spectral range dominated by the 1-alkyl-3-methylimidazolium Raman modes. No essential perturbation of the $[C_nC_1Im]^+$ cation Raman bands could be resolved (except for a rather weak blue shift (1−2 cm^{-1}) of the C(4,5)−H stretching mode at high frequencies), in agreement with previous studies reporting the absence of pronounced variations of the cation vibrational bands in aqueous mixtures of fluorinated $[C_nC_1Im][BF_4]/[PF_6]$ ILs.[24,25,40,60−63]

On the other hand, the $[TCM]^-$ Raman modes presented a marked variation with increasing water content, especially the CC and CN stretches as illustrated in Figure 10c and 10d for $[C_4C_1Im][TCM]/H_2O$ (the corresponding Raman spectra for $[C_8C_1Im][TCM]/H_2O$ are shown in Figure S5, Supporting Information). Specifically, the symmetric CC and both the

dx.doi.org/10.1021/jp407364e | J. Phys. Chem. B 2013, 117, 12234−12251

symmetric and the antisymmetric CN stretching modes presented a continuous shift to higher frequencies along with broadening as the H_2O molar fraction increases, while the in-plane CCN bending mode exhibited considerable broadening with only a minor shift on the order of 1 cm^{-1}, as shown in Figure 11. The consequent hardening of the CC and CN modes that shifted toward the free anion positions (Table 3) points to the strengthening of the corresponding bonds by introduction of water molecules that disrupt the $[C_nC_1Im]^+$–$[TCM]^-$ coupling.

This behavior can be effectively explained by the hydrogen bonding of water molecules with two discrete anions leading to formation of symmetric A···H–O–H···A structures, as originally put forward by Cammarata et al.[24] and recently elaborated by Danten et al.,[25] where weak shifts (<5 cm^{-1}) of the anion symmetric stretching modes have been explicitly predicted. However, the anticipated charge delocalization in the $[TCM]^-$ anion[53] may modify the form of the TCM–H_2O bonding compared to the nearly symmetric complexes dictated by the strong F···H–O hydrogen bonds in fluorinated ILs.[25] In fact, a very recent study of the hydration dynamics of $[TCM]^-$ anions indicated that water molecules may be H bonded to the tricyanomethanide anions both through the nitrile groups that may lead to symmetry lowering by bending the C–C–N bond as well as via the central carbon atom.[64]

A more subtle hydration scheme can be then inferred that may account for the continuous broadening underlying the CC and CN stretches as well as the CCN bending mode with the increase of the H_2O content (Figure 11). To this end, it is very interesting to note that the antisymmetric CN stretch for the dry ILs exhibits a rather asymmetric line shape that cannot be accurately fit to a single profile of any form (Lorentzian, Gaussian, or Voight), as shown in Figure 12. This could be rationalized by small deviations from the planar D_{3h} symmetry due to the possible bending of $[TCM]^-$ ions atop the imidazolium ring,[65,66] resulting in activation of two close-lying CN modes that can readily fit the observed asymmetric profile of this mode. On the other hand, the profile of the antisymmetric CN mode becomes considerably more symmetric in the highly hydrated mixtures (Figure 12), indicating that H_2O molecules, most likely situated between two tricyanomethanide anions, effectively release these symmetry deviations by compensating for the strong TCM–imidazolium bonding.

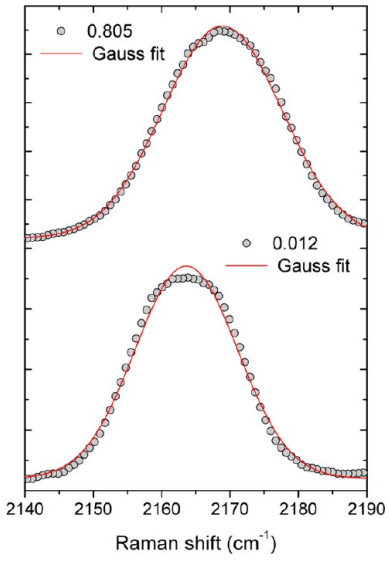

Figure 12. Fitting of the antisymmetric CN stretching mode with a single Gaussian line shape for 0.012 and 0.805 H_2O molar fractions of $[C_4C_1im][TCM]/H_2O$.

Tertiary TCM IL/H_2O/CO_2 Mixtures. Figure 13 shows characteristic Raman spectra of $[C_4C_1im][TCM]/H_2O$ mixtures before and after absorption of CO_2 at 278 K and a pressure of 10 bar (corresponding Raman spectra for $[C_8C_1Im][TCM]/H_2O$ are shown in Figure S6, Supporting Information). At low H_2O concentrations, no essential difference compared to the dry IL could be detected, i.e., the Fermi dyad emerged at the same peak positions as for the dry IL with no distortion of the anion/cation Raman bands. However, at high H_2O molar fractions a weak but clear red shift by ca. 1–2 cm^{-1} of the symmetric CC as well as both the symmetric and the antisymmetric CN stretching modes was observed (the in-plane CCN bending mode remained unaffected) toward the corresponding frequencies at lower H_2O contents. A clear tendency of the heavily hydrated IL liquid to restore the original positions of the tricyanomethanide CC and CN stretches determined by the anion–cation interaction of the dry system was accordingly inferred upon CO_2 dissolution. Specifically, a decrease of the water content in the IL/H_2O system by 0.1–0.2% H_2O molar fraction in the presence of dissolved CO_2 could justify the observed softening of the CC and CN stretches and the concomitant strengthening of the $[C_nC_1im]^+$–$[TCM]^-$ coupling. This distinctive feature of the ternary $[C_nC_1Im][TCM]/H_2O/CO_2$ system further implies a subtle competition between the TCM–H_2O and the TCM–CO_2 interactions in contrast to the anion fluorinated ILs, whose strong propensity to strong double hydrogen-bonded F···H–O–H···F complexes leads to rather weak effects of water on their CO_2 absorption capacity.

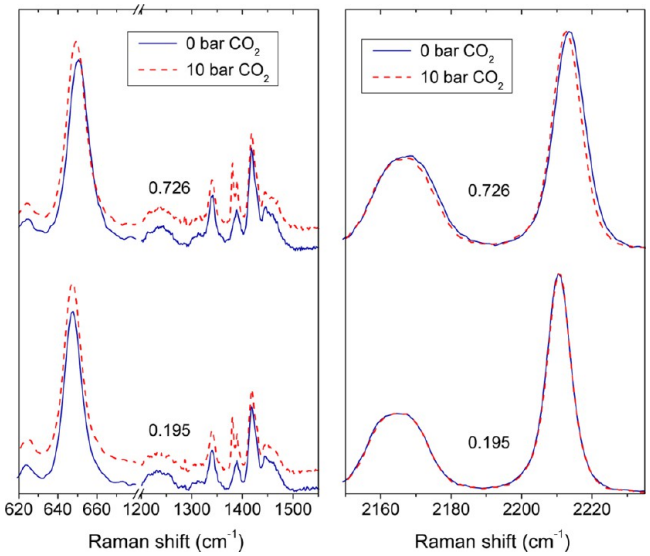

Figure 13. Raman spectra for $[C_4C_1im][TCM]/H_2O$ at 0.195 and 0.726 water molar fractions before and after absorption of CO_2 under a pressure of 10 bar at 278 K.

3.6. Molecular Exchange Mechanism in TCM IL/H_2O/CO_2 Mixtures.

Relying on the combined analysis of the experimental data on the excess molar volume and viscosity deviations, CO_2 absorption/kinetics, and Raman spectroscopy,

dx.doi.org/10.1021/jp407364e | J. Phys. Chem. B 2013, 117, 12234–12251

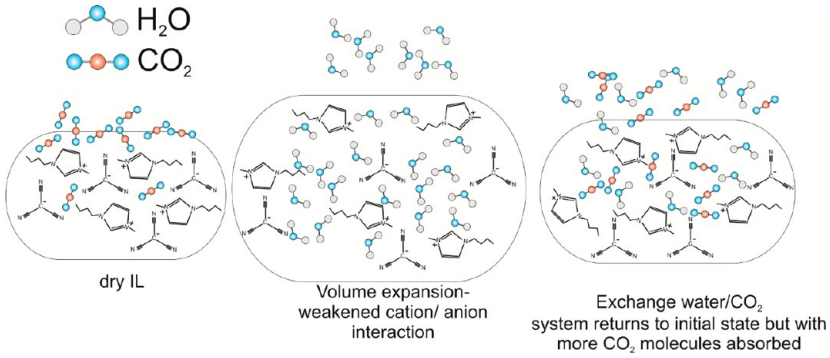

Figure 14. Schematic presentation of the molecular exchange mechanism underlying the enhanced CO_2 absorption in the hybrid $[C_nC_1im][TCM]/H_2O$ solvents.

we concluded a CO_2 absorption/H_2O displacement mechanism that underlies the unique enhancement of CO_2 solubility in the hybrid $[C_nC_1Im][TCM]/H_2O$ solvents, schematically illustrated in Figure 14. In the dry IL, CO_2 absorption is mainly limited by the restricted free space to be occupied by CO_2 molecules that may weakly interact with the $[TCM]^-$ anions. Mixing of the ionic liquid with water disrupts the anion−cation interactions through formation of hydrogen-bonded TCM−H_2O complexes, resulting in the increase of the free volume for the binary solvent. Thereby, CO_2 molecules attain easier and higher accessibility to unoccupied free sites, which is expressed by 10−100-fold faster absorption rates. In turn, the presence of CO_2 effectively breaks the water/IL interactions due to the competition of TCM−H_2O and TCM−CO_2 interactions leading to H_2O desorption. In this way the system seems to return to its initial state though at a greatly enhanced CO_2 load, which is 4−5 times higher compared to the dry IL.

4. CONCLUSIONS

A gravimetric study of CO_2 and H_2O absorption in 1-alkyl-3-methylimidazoliun tricyanomethanide, $[C_nC_1im][TCM]$ (n = 4, 8), ILs revealed a significant enhancement of both the CO_2 solubility and the diffusivity in binary $[C_nC_1im][TCM]/H_2O$ systems compared to dry solvents, providing a marked improvement over most physically and chemically CO_2 absorbing ILs, where water commonly impairs their CO_2 capture efficiency.

In-situ Raman spectroscopy on the dry $[C_nC_1im][TCM]/CO_2$ systems at different temperatures showed that CO_2 is physically absorbed in the TCM ILs without distorting the ILs local structure, in agreement with the reversible CO_2 absorption/desorption isotherms for the dry ILs. This was directly evidenced by the negligible effects of CO_2 absorption on the anion/cation Raman bands of $[C_nC_1im][TCM]$, in contrast to the distinct red shift and broadening of the CO_2 Fermi resonance dyad and the systematic increase of its relative intensity with the alkyl chain length and the decrease of temperature. Mixing of $[C_nC_1im][TCM]$ ILs with water within their miscibility regions, determined by the corresponding alkyl chain length, resulted in positive excess molar volumes and negative viscosity deviations for the binary aqueous systems that followed a nonmonotonous dependence on the water molar fractions, characteristic of the perturbation of the ILs organization by the water molecules. This variation was accompanied by a prominent blue shift of the tricyanomethanide CC and CN stretching Raman modes with the increase of water content in $[C_nC_1im][TCM]/H_2O$, reflecting the disruption of the $[C_nC_1im]^+$−$[TCM]^-$ coupling by water molecules hydrogen bonded to the tricyanomethanide anions. Gravimetric measurements of the transient CO_2 absorption kinetics revealed a pronounced pressure and IL depended maximum for the hybrid IL/H_2O solvents pointing to desorption of H_2O molecules. This was further corroborated by in-situ Raman measurements in the tertiary $[C_nC_1im]$-$[TCM]/H_2O/CO_2$ mixtures, where a tendency of the $[TCM]^-$ Raman modes to restore their original (dry IL) positions was traced for high water contents.

A molecular exchange mechanism between CO_2 in the gas phase and H_2O in the liquid phase was accordingly implicated to explain the enhanced CO_2 absorption in the hybrid solvents. Dilution of water above a certain concentration in the $[C_nC_1im][TCM]$ ILs results in expansion of the IL's free volume via the intervening water molecules that interact with the $[TCM]^-$ anions, providing higher and faster (10−100-fold increase of the CO_2 absorption rates) accessibility of CO_2 molecules to the ILs void space. Furthermore, the presence of appreciable amounts of CO_2 effectively breaks the IL−H_2O coupling due to the competing TCM−H_2O and TCM−CO_2 interactions, triggering desorption of H_2O from ionic liquid that tends to restore its initial state, accommodating a significantly higher amount (4−5 times increased) of CO_2. Combination of the enhanced CO_2 absorption capacity of $[C_nC_1im][TCM]/H_2O$ binary systems with high thermal stability, low viscosity, and scalable synthesis of the neat $[C_nC_1im][TCM]$ ILs makes these hybrid solvents very promising for CO_2 capture applications.

■ ASSOCIATED CONTENT

Supporting Information

Tables with numerical data on the excess molar volumes, density, Redlich−Kister correlation coefficients, viscosity, viscosity deviations of neat $[C_nC_1im][TCM]$ and the corresponding IL/H_2O binary systems; Raman spectra and intensity ratios (I_{1380}/I_{646}) for $[C_nC_1im][TCM]/CO_2$ at different temperatures and as a function of the alkyl chain length; variation of the $[TCM]^-$ Raman modes with the water concentration for $[C_8C_1im][TCM]/H_2O$ and Raman spectra of $[C_4C_1im][TCM]/H_2O/CO_2$. This material is available free of charge via the Internet at http://pubs.acs.org.

■ AUTHOR INFORMATION

Corresponding Author

*E-mail: groman@chem.demokritos.gr.

Notes

The authors declare no competing financial interest.

■ ACKNOWLEDGMENTS

The authors gratefully acknowledge support by the IOLICAP (grant agreement no. 283077), EU FP7 project.

■ REFERENCES

(1) Seddon, K. R. J. Ionic Liquids for Clean Technology. *Chem. Technol. Biotechnol.* **1997**, *68*, 351−356.
(2) Wasserscheid, P.; Welton, T. *Ionic Liquids in Synthesis*; Wiley-VCH: New York, 2008; Vol. 2.
(3) Blanchard, L. A.; Hancu, D.; Beckman, E. J.; Brennecke, J. F. Green Processing Using Ionic Liquids and CO_2. *Nature* **1999**, *399*, 28−29.
(4) Bara, J. E.; Camper, D. E.; Gin, D. L.; Noble, R. D. Room-Temperature Ionic Liquids and Composite Materials: Platform Technologies for CO_2 Capture. *Acc. Chem. Res.* **2010**, *43*, 152−159.
(5) Brennecke, J. F.; Gurkan, B. E. Ionic Liquids for CO_2 Capture and Emission Reduction. *J. Phys. Chem. Lett.* **2010**, *1*, 3459−3464.
(6) Ramdin, M.; de Loos, T. W.; Vlugt, T. J. H. State-of-the-Art of CO_2 Capture with Ionic Liquids. *Ind. Eng. Chem. Res.* **2012**, *51*, 8149−8177.
(7) Aki, S. N. V. K.; Mellein, B. R.; Saurer, E. M.; Brennecke, J. F. High-Pressure Phase Behavior of Carbon Dioxide with Imidazolium-Based Ionic Liquids. *J. Phys. Chem. B* **2004**, *108*, 20355−20365.
(8) Zhang, Z. F.; Wu, W. Z.; Gao, H. X.; Han, B. X.; Wang, B.; Huang, Y. Tri-phase Behavior of Ionic Liquid−Water−CO_2 System at Elevated Pressures. *Phys. Chem. Chem. Phys.* **2004**, *6*, 5051−5055.
(9) Fu, D. B.; Sun, X. W.; Pu, J. J.; Zhao, S. Q. Effect of Water Content on the Solubility of CO_2 in the Ionic Liquid [bmim][PF_6]. *J. Chem. Eng. Data* **2006**, *51*, 371−375.
(10) Andanson, J.-M.; Jutz, F.; Baiker, A. Investigation of Binary and Ternary Systems of Ionic Liquids with Water and/or Supercritical CO_2 by in Situ Attenuated Total Reflection Infrared Spectroscopy. *J. Phys. Chem. B* **2010**, *114*, 2111−2117.
(11) Taib, M. M.; Murugesan, T. Solubilities of CO_2 in Aqueous Solutions of Ionic Liquids (ILs) and Monoethanolamine (MEA) at Pressures from 100 to 1600 kPa. *Chem. Eng. J.* **2012**, *181−182*, 56−62.
(12) Goodrich, B. F.; De La Fuente, J. C.; Gurkan, B. E.; Lopez, Z. K.; Price, E. A.; Huang, Y.; Brennecke, J. F. Effect of Water and Temperature on Absorption of CO_2 by Amine-Functionalized Anion-Tethered Ionic Liquids. *J. Phys. Chem. B* **2011**, *115*, 9140−9150.
(13) Stevanovic, S.; Podgorsek, A.; Padua, A. A. H.; Gomes, M. F. C. Effect of Water on the Carbon Dioxide Absorption by 1-Alkyl-3-methylimidazolium Acetate Ionic Liquids. *J. Phys. Chem. B* **2012**, *116*, 14416−14425.
(14) Perez-Blanco, M. E.; Maginn, E. J. Molecular Dynamics Simulations of Carbon Dioxide and Water at an Ionic Liquid Interface. *J. Phys. Chem. B* **2011**, *115*, 10488−10499.
(15) Bates, E. D.; Mayton, R. D.; Ntai, I.; Davis, J. H. CO_2 Capture by a Task-Specific Ionic Liquid. *J. Am. Chem. Soc.* **2002**, *124*, 926−927.
(16) Gurkan, B. E.; de la Fuente, J. C.; Mindrup, E. M.; Ficke, L. E.; Goodrich, B. F.; Price, E. A.; Schneider, W. F.; Brennecke, J. F. Equimolar CO_2 Absorption by Anion-Functionalized Ionic Liquids. *J. Am. Chem. Soc.* **2010**, *132*, 2116−211.
(17) Gurkan, B.; Goodrich, B. F.; Mindrup, E. M.; Ficke, L. E.; Massel, M.; Seo, S.; Senftle, T. P.; Wu, H.; Glaser, M. F.; Shah, J. K.; et al. Molecular Design of High Capacity, Low Viscosity, Chemically Tunable Ionic Liquids for CO_2 Capture. *J. Phys. Chem. Lett.* **2010**, *1*, 3494−3499.
(18) Goodrich, B. F.; de la Feunte, J. C.; Gurkan, B. E.; Zadigan, D. J.; Price, E. A.; Huang, Y.; Brennecke, J. F. Experimental Measurements of Amine-Functionalized Anion-Tethered Ionic Liquids with Carbon Dioxide. *Ind. Eng. Chem. Res.* **2011**, *50*, 111−118.
(19) Feng, Z.; Gang, F. C.; Ting, W. Y.; Tao, W. Y.; Mina, L. A.; Bing, Z. Z. Absorption of CO_2 in the Aqueous Solutions of Functionalized Ionic Liquids and MDEA. *Chem. Eng. J.* **2010**, *160*, 691−697.
(20) Zhang, Y.; Yu, P.; Luo, Y. Absorption of CO_2 by Amino Acid-Functionalized and Traditional Dicationic Ionic Liquids: Properties, Henry's Law Constants and Mechanisms. *Chem. Eng. J.* **2013**, *214*, 355−363.
(21) Gutowski, K. E.; Maginn, E. J. Amine-Functionalized Task-Specific Ionic Liquids: A Mechanistic Explanation for the Dramatic Increase in Viscosity upon Complexation with CO_2 from Molecular Simulation. *J. Am. Chem. Soc.* **2008**, *130*, 14690−14704.
(22) Kazarian, S. G.; Briscoe, B. J.; Welton, T. Combining Ionic Liquids and Supercritical Fluids: in Situ ATR-IR Study of CO_2 Dissolved in Two Ionic Liquids at High Pressures. *Chem. Commun.* **2000**, 2047−2048.
(23) Cadena, C.; Anthony, J. L.; Shah, J. K.; Morrow, T. I.; Brennecke, J. F.; Maginn, E. J. Why Is CO_2 So Soluble in Imidazolium-Based Ionic Liquids? *J. Am. Chem. Soc.* **2004**, *126*, 5300−5308.
(24) Cammarata, L.; Kazarian, S. G.; Salter, P. A.; Welton, T. Molecular States of Water in Room Temperature Ionic Liquids. *Phys. Chem. Chem. Phys.* **2001**, *3*, 5192−5200.
(25) Danten, Y.; Cabaco, M. I.; Besnard, M. Interaction of Water Highly Diluted in 1-Alkyl-3-methyl Imidazolium Ionic Liquids with the PF_6^- and BF_4^- Anions. *J. Phys. Chem. A* **2009**, *113*, 2873−2889.
(26) Danten, Y.; Cabaco, M. I.; Besnard, M. Interaction of Water Diluted in 1-Butyl-3-methyl Imidazolium Ionic Liquids by Vibrational Spectroscopy Modeling. *J. Mol. Liq.* **2010**, *153*, 57−66.
(27) Forsyth, S. A.; Stuart, R.; Batten; Qing Dai; MacFarlane, D. R. Ionic Liquids Based on Imidazolium and Pyrrolidinium Salts of the Tricyanomethanide Anion. *Aust. J. Chem.* **2004**, *57*, 121−124.
(28) Brand, H.; Liebman, J. F.; Schulz, A.; Mayer, P.; Villinger, A. Nonlinear, Resonance-Stabilized Pseudohalides: From Alkali Methanides to Ionic Liquids of Methanides. *Eur. J. Inorg. Chem.* **2006**, 4294−4308.
(29) Yoshida, Y.; Muroi, K.; Otsuka, A.; Saito, G.; Takahashi, M.; Yoko, T. 1-Ethyl-3-methylimidazolium Based Ionic Liquids Containing Cyano Groups: Synthesis, Characterization, and Crystal Structure. *Inorg. Chem.* **2004**, *43*, 1458−1462.
(30) Labropoulos, A. I.; Romanos, G. Em.; Kouvelos, E.; Falaras, P.; Likodimos, V.; Francisco, M.; Kroon, M. C.; Iliev, B.; Adamova, G.; Schubert, T. J. S. Alkyl-methylimidazolium Tricyanomethanide Ionic Liquids under Extreme Confinement onto Nanoporous Ceramic Membranes. *J. Phys. Chem. C* **2013**, *117*, 10114−10127.
(31) Hong, G.; Jacquemin, J.; Husson, P.; Costa Gomes, M. F.; Deetlefs, M.; Nieuwenhuyzen, M.; Sheppard, O.; Hardacre, C. Effect of Acetonitrile on the Solubility of Carbon Dioxide in 1-Ethyl-3-methylimidazolium Bis(trifluoromethylsulfonyl)amide. *Ind. Eng. Chem. Res.* **2006**, *45*, 8180−8188.
(32) Jacquemin, J.; Costa Gomes, M. F.; Husson, P.; Majer, V. Solubility of Carbon Dioxide, Ethane, Methane, Oxygen, Nitrogen, Hydrogen, Argon, and Carbon Monoxide in 1-Butyl-3-methylimidazolium Tetrafluoroborate Between Temperatures 283 and 343 K and at Pressures Close to Atmospheric. *J. Chem. Thermodyn.* **2006**, *38*, 490−502.
(33) Sakellarios, N. I.; Kazarian, S. G. Situ IR Spectroscopic Study of the CO_2-induced Swelling of Ionic Liquid Media. *ACS Symp. Ser.* **2005**, *901*, 89−10.
(34) Redlich, O.; Kister, A. T. Algebraic Representation of Thermodynamic Properties and the Classification of Solutions. *Ind. Eng. Chem.* **1948**, *40*, 345−348.
(35) Carvalho, P. J.; Regueira, T.; Santos, L. M. N. B. F.; Fernandez, J.; Coutinho, J. A. P. Effect of Water on the Viscosities and Densities of 1-Butyl-3-methylimidazolium Dicyanamide an 1-Butyl-3-methylimidazolium Tricyanomethane at Atmospheric Pressure. *J. Chem. Eng. Data* **2010**, *55*, 645−652.
(36) Prolongo, M. G.; Masegosa, R. M.; Hernández-Fuentes, I.; Horta, A. Viscosities and Excess Volumes of Binary Mixtures Formed by the Liquids Acetonitrile, Pentyl Acetate, 1-Chlorobutane, and Carbon Tetrachloride at 25 °C. *J. Phys. Chem.* **1984**, *88*, 2163−2167.

(37) Canongia Lopes, J. N.; Pádua, A. A. Nanostructural Organization in Ionic Liquids. *J. Phys. Chem. B* **2006**, *110*, 3330−3335.
(38) Triolo, A.; Russina, O.; Bleif, H. J.; Di Cola, E. Nanoscale Segregation in Room Temperature Ionic Liquids. *J. Phys. Chem. B* **2007**, *111*, 4641−4644.
(39) Jiang, W.; Wang, Y. T.; Voth, G. A. Molecular Dynamics Simulation of Nanostructural Organization in Ionic Liquid/Water Mixtures. *J. Phys. Chem. B* **2007**, *111*, 4812−4818.
(40) Fazio, B.; Triolo, A.; Di Marco, G. Local Organization of Water and its Effect on the Structural Heterogeneities in Room-Temperature Ionic Liquid/H_2O Mixtures. *J. Raman Spectrosc.* **2008**, *39*, 233−237.
(41) García-Miaja, G.; Troncoso, J.; Romani, L. Excess Enthalpy, Density, and Heat Capacity for Binary Systems of Alkylimidazolium-based Ionic Liquids + Water. *J. Chem. Thermodyn.* **2009**, *41*, 161−166.
(42) Ortega, J.; Vreekamp, R.; Marrero, E.; Penco, E. Thermodynamic Properties of 1-Butyl-3-Methylpyridinium Tetrafluoroborate and Its Mixtures with Water and Alkanols. *J. Chem. Eng. Data* **2007**, *52*, 2269−2276.
(43) Gill, D. S.; Cheema, T. S. Preferential Solvation of Ions in Mixed Solvents. 1. Conductance and Viscosity Measurements of Electrolytes in N,N-Dimethylformamide + Acetonitrile mixtures at 25 °C. *Z. Phys. Chem (N. F.)* **1983**, *134*, 205−214.
(44) Marcus, Y. *Ion Solvation*; Wiley: New York, 1985.
(45) Fort, R. J.; Moore, W. R. Viscosities of Binary Liquid Mixtures. *Trans. Faraday Soc.* **1966**, *62*, 1112−1119.
(46) Talaty, R.; Raja, S.; Storhaug, V. J.; Dölle, A.; Carper, W. R. Raman and Infrared Spectra and ab Initio Calculations of C_{2-4}MIM Imidazolium Hexafluorophosphate Ionic Liquids. *J. Phys. Chem. B* **2004**, *108*, 13177−13184.
(47) Berg, R. W.; Deetlefs, M.; Seddon, K. R.; Shim, I.; Thompson, J. M. Raman and ab Initio Studies of Simple and Binary 1-Alkyl-3-methylimidazolium Ionic Liquids. *J. Phys. Chem. B* **2005**, *109*, 19018−19025.
(48) Heimer, N. E.; Sesto, R. E. D.; Meng, Z.; Wilkes, J. S.; Carper, W. R. Vibrational Spectra of Imidazolium Tetrafluoroborate Ionic Liquids. *J. Mol. Liq.* **2006**, *124*, 84−95.
(49) Rivera-Rubero, S.; Baldelli, S. Surface Characterization of 1-Butyl-3-methylimidazolium Br^-, I^-, PF_6^-, BF_4^-, $(CF_3SO_2)_2N^-$, SCN^-, $CH_3SO_3^-$, $CH_3SO_4^-$, and $(CN)_2N^-$ Ionic Liquids by Sum Frequency Generation. *J. Phys. Chem. B* **2006**, *110*, 4756−4765.
(50) Holomb, R.; Martinelli, A.; Albinsson, I.; Lassègues, J. C.; Johansson, P.; Jacobsson, P. Ionic Liquid Structure: the Conformational Isomerism in 1-Butyl-3-methyl-imidazolium Tetrafluoroborate ([bmim][BF_4]). *J. Raman Spectrosc.* **2008**, *39*, 793−805.
(51) Kiefer, J.; Pye, C. C. Structure of the Room-Temperature Ionic Liquid 1-Hexyl-3-methylimidazolium Hydrogen Sulfate: Conformational Isomerism. *J. Phys. Chem. A* **2010**, *114*, 6713−6720.
(52) Hipps, K. W.; Aplin, A. T. The Tricyanomethanide Ion: An Infrared, Raman, and Tunneling Spectroscopy Study Including Isotopic Substitution. *J. Phys. Chem.* **1985**, *89*, 5459−5464.
(53) Dixon, D. A.; Calabrese, J. C.; Miller, J. S. Crystal and Molecular Structure of the Charge Transfer Salt of Decamethylferrocenium and Tricyanomethanide: $[Fe(C_5Me_5)_2]^+\cdot C([CN)_3]^-$. The Electronic Structure and Spectra of $[C(CN)_3]^-$. *J. Am. Chem. Soc.* **1986**, *108*, 2582−2588.
(54) Weidinger, D.; Houchins, C.; Owrutsky, J. C. Vibrational dynamics of tricyanomethanide. *Chem. Phys. Lett.* **2012**, *60*, 525−526.
(55) Koddermann, T.; Wertz, C.; Heintz, A.; Ludwig, R. Ion-Pair Formation in the Ionic Liquid 1-Ethyl-3-methylimidazolium Bis-(triflyl)imide as a Function of Temperature and Concentration. *Chem. Phys. Chem.* **2006**, *7*, 1944−1949.
(56) Grondin, J.; Lassègues, J.-C.; Cavagnat, D.; Buffeteau, T.; Johansson, P.; Holomb, R. Revisited vibrational assignments of imidazolium-based ionic liquids. *J. Raman Spectrosc.* **2011**, *42*, 733−743.
(57) Cabaco, M. I.; Besnard, M.; Danten, Y.; Coutinho, J. A. P. Solubility of CO_2 in 1-Butyl-3-methyl-imidazolium-trifluoro Acetate Ionic Liquid Studied by Raman Spectroscopy and DFT Investigations. *J. Phys. Chem. B* **2011**, *115*, 3538−3550.
(58) Anderson, G. A. The Raman Spectra of Carbon Dioxide in Liquid H_2O and D_2O. *J. Phys. Chem.* **1977**, *81*, 273−276.
(59) Makino, T. In situ Raman Study of Dissolved Carbon-Dioxide Induced Changes of Imidazolium-Based Ionic Liquids. *J. Phys.: Conf. Ser.* **2010**, *215*, 012068.
(60) Jeon, Y.; Sung, J.; Kim, D.; Seo, C.; Cheong, H.; Ouchi, Y.; Wawa, R.; Hamaguchi, H. O. Structural Change of 1-Butyl-3-methylimidazolium Tetrafluoroborate + Water Mixtures Studied by Infrared Vibrational Spectroscopy. *J. Phys. Chem. B* **2008**, *112*, 923−928.
(61) Gao, Y.; Zhang, L. Q.; Wang, Y.; Li, H. R. Probing Electron Density of H-Bonding between Cation-Anion of Imidazolium-Based Ionic Liquids with Different Anions by Vibrational Spectroscopy. *J. Phys. Chem. B* **2010**, *114*, 2828−2833.
(62) MacMillan, A. C.; McIntire, T. M.; Freites, J. A.; Tobias, D. J.; Nizkorodov, S. A. Interaction of Water Vapor with the Surfaces of Imidazolium-Based Ionic Liquid Nanoparticles and Thin Films. *J. Phys. Chem. B* **2012**, *116*, 11255−11265.
(63) Schenk, J.; Panne, U.; Albrecht, M. Interaction of Levitated Ionic Liquid Droplets with Water. *J. Phys. Chem. B* **2012**, *116*, 14171−14177.
(64) Kuroda, D. G.; Singh, P. K.; Hochstrasser, R. M. Differential Hydration of Tricyanomethanide Observed by Time Resolved Vibrational Spectroscopy. *J. Phys. Chem. B* **2013**, *117*, 4354−4364.
(65) Emel'yanenko, V. N.; Zaitsau, D. H.; Verevkin, S. P.; Heintz, A.; Voß, K.; Schulz, A. Vaporization and Formation Enthalpies of 1-Alkyl-3-methylimidazolium Tricyanomethanides. *J. Phys. Chem. B* **2011**, *115*, 11712−11717.
(66) Peñalber, C. Y.; Grenoble, Z.; Baker, G. A.; Baldelli, S. Surface Characterization of Imidazolium-Based Ionic Liquids with Cyano-functionalized Anions at the Gas-Liquid Interface Using Sum Frequency Generation Spectroscopy. *Phys. Chem. Chem. Phys.* **2012**, *14*, 5122−5131.